

**MULTILAYER ANTENNA ARRAYS FOR ENVIRONMENTAL  
SENSING APPLICATIONS**

A Thesis  
Presented to  
The Academic Faculty

by

Ana Maria Yepes

In Partial Fulfillment  
of the Requirements for the Degree  
Masters of Science in the  
School of Electrical and Computer Engineering

Georgia Institute of Technology  
August, 2010

**MULTILAYER ANTENNA ARRAYS FOR ENVIRONMENTAL  
SENSING APPLICATIONS**

Approved by:

Dr. John Papapolymerou, Advisor  
School of Electrical and Computer Engineering  
*Georgia Institute of Technology*

Dr. John D. Cressler  
School of Electrical and Computer Engineering  
*Georgia Institute of Technology*

Dr. Emmanouil Tentzeris  
School of Electrical and Computer Engineering  
*Georgia Institute of Technology*

Date Approved: May 21, 2010

To My Parents

## **ACKNOWLEDGEMENTS**

I would like to thank the NASA Earth-Sun System Technology Office for supporting this research. Special thanks to Professor John Papapolymerou for his academic guidance and to the members of the MircTech group and GTRI for their assistance on this research. I would also like to thank my family and friends for their support.

# TABLE OF CONTENTS

	Page
ACKNOWLEDGEMENTS	iv
LIST OF TABLES	viii
LIST OF FIGURES	ix
SUMMARY	xii
<u>CHAPTER</u>	
1 INTRODUCTION	1
1.1 Overview of Antennas	1
1.2 Fundamental Parameters of Antennas	2
1.3 The Research Presented	3
2 BACKGROUND	5
2.1 Microstrip Antenna Modeling	8
2.2 Feeding Methods	11
2.2.1 Aperture Coupling Feed	11
2.2.2 Via Feed	12
2.3 Microstrip Antenna Arrays	13
2.3.1 N-Element Uniform Linear Array	14
2.3.2 Feed Networks	16
2.3.2.1 T-Junction Power Divider	17
2.3.2.1 Wilkinson Power Divider	19
3 DESIGN AND SIMULATION OF ANTENNA ARRAYS	21
3.1 Substrate Material	21
3.1.1 ULTRALAM 3850 Laminate	22

3.1.2	RT/Duroid® 5880LZ Laminate	23
3.2	Antenna Arrays with Corporate Feed Networks using T-Junctions	24
3.2.1	Aperture-Coupled Antenna Arrays	27
3.2.1.1	Antenna Arrays using ULTRALAM 3850	28
3.2.1.2	Antenna Arrays using RT/Duroid® 5880LZ	30
3.2.2	Via-Fed Antenna Arrays	33
3.3	Antenna Arrays with Corporate Feed Networks using Wilkinson Dividers	36
3.3.1	X-Band Antenna Arrays	39
3.3.1.1	Antenna Arrays using ULTRALAM 3850	39
3.3.1.2	Antenna Arrays using RT/Duroid® 5880LZ	40
3.3.2	Ka-Band Antenna Arrays	43
3.4	Antenna Phased Array Beam Steering	45
4	FABRICATION AND MEASUREMENT RESULTS	47
4.1	Fabrication	47
4.2	Measurement Results	50
4.2.1	Measured Results for Arrays using ULTRALAM 3850	51
4.2.2	Measured Results for Arrays using RT/Duroid® 5880LZ	53
4.2.2.1	Antenna Arrays with Feed Networks using T-Junctions	53
4.2.2.2	Antenna Arrays with Feed Networks using Wilkinson Dividers	56
4.2.3	Antenna Array Beam Steering	58
5	ANTENNA ARRAYS APPLICATIONS AND CONCLUSIONS	59
5.1	Antenna Arrays in Environmental Sensing	59
5.2	Conclusions	60

APPENDIX A: Electrical Properties of LCP vs. Other Laminates	63
APPENDIX B: Predicted Beam Steering of 8x8 Array for Different Phase Shift Values	64
REFERENCES	65

## LIST OF TABLES

	Page
Table 1: Properties of ULTRALAM 3850 Laminate	23
Table 2: Properties of RT/Duroid® 5880LZ Laminate	24
Table 3: Dimensions for 8x1 Array with T-Junctions using ULTRALAM 3850	30
Table 4: Simulation Results for Arrays with Aperture Coupling and T-Junctions using ULTRALAM 3850	30
Table 5: Dimensions for 8x8 Array with T-Junctions using RT/Duroid® 5880LZ	33
Table 6: Simulation Results for Arrays with Aperture Coupling and T-Junctions using RT/Duroid® 5880LZ	33
Table 7: Dimensions for 8x8 Array with Via Feed using RT/Duroid® 5880LZ	36
Table 8: Simulation Results for 8x8 Array with Via Feed	36
Table 9: Dimensions for X-Band 8x1 Array with Wilkinson Dividers using ULTRALAM 3850	40
Table 10: Simulation Results for X-Band 8x1 Array with Wilkinson Dividers using ULTRALAM 3850	40
Table 11: Dimensions for X-Band 8x8 Array with Wilkinson Dividers using RT/Duroid® 5880LZ	42
Table 12: Simulation Results for X-Band Arrays with Wilkinson Dividers using RT/Duroid® 5880LZ	42
Table 13: Dimensions for Ka-Band 4x4 Array with Wilkinson Dividers using RT/Duroid® 5880LZ	44
Table 14: Simulation Results for Ka-Band Arrays with Wilkinson Dividers using RT/Duroid® 5880LZ	45
Table 15: Values of Phase Shift $\alpha$ Obtained from Phase Shifter	46

## LIST OF FIGURES

	Page
Figure 1: Microstrip antenna.	6
Figure 2: Transmission model equivalent of microstrip patch.	9
Figure 3: Fringing effect on length of patch.	10
Figure 4: Aperture-coupled feed and its equivalent circuit.	12
Figure 5: Via feed and its equivalent circuit.	13
Figure 6: Far-field geometry of n-element array with elements uniformly spaced along the x-axis.	15
Figure 7: Feed network arrangements for microstrip patch arrays.	17
Figure 8: Transmission Line Model of a lossless T-junction.	18
Figure 9: Quarter-wave matching transformer.	19
Figure 10: Equivalent transmission line circuit of equal-split Wilkinson power divider.	19
Figure 11: Cross-sectional view of substrate stack-up for X-band antenna arrays.	25
Figure 12: Layout of reactive T-junction used in RF feed networks.	27
Figure 13: Layout of 4x1 array with aperture coupling and T-junctions (ULTRALAM).	29
Figure 14: Simulated return loss and radiation pattern of 4x1 array with aperture coupling and T-junctions.	29
Figure 15: Layout of 8x1 array with aperture coupling and T-junctions (ULTRALAM).	29
Figure 16: Simulated return loss and radiation pattern of 8x1 array with aperture coupling and T-junctions (ULTRALAM).	29
Figure 17: Layout of 4x1 array with aperture coupling and T-junctions (RT/Duroid).	31
Figure 18: Simulated return loss and radiation pattern of 4x1 array with aperture coupling and T-junctions (RT/Duroid).	31
Figure 19: Layout of 8x2 array with aperture coupling and T-junctions (RT/Duroid).	31

Figure 20: Simulated return loss and radiation pattern of 8x2 array with aperture coupling and T-junctions (RT/Duroid).	31
Figure 21: Layout of 8x8 array with aperture coupling and T-junctions (RT/Duroid).	32
Figure 22: Simulated return loss and radiation pattern of 8x8 array with aperture coupling and T-junctions (RT/Duroid).	32
Figure 23: Substrate stack-up for via-fed arrays.	34
Figure 24: Layout of 8x8 array with via feed.	35
Figure 25: Simulation return loss and radiation pattern of 8x8 array with via feed.	35
Figure 26: Substrate stack-up for aperture coupled antenna arrays.	37
Figure 27: Layout of Wilkinson divider used in embedded RF feed network.	38
Figure 28: Layout of X-band 8x1 array with Wilkinson dividers (ULTRALAM).	39
Figure 29: Simulated return loss and radiation pattern of X-band 8x1 array with Wilkinson dividers. (ULTRALAM).	39
Figure 30: Layout of X-band 4x1 array with Wilkinson dividers (RT/Duroid).	40
Figure 31: Simulated return loss and radiation pattern of X-band 4x1 array with Wilkinson dividers (RT/Duroid).	41
Figure 32: Layout of X-band 8x8 array with Wilkinson dividers (RT/Duroid).	41
Figure 33: Simulated return loss and radiation pattern of X-band 8x8 array with Wilkinson dividers. (RT/Duroid).	42
Figure 34: Cross-sectional view of substrate stack-up used for Ka-band arrays.	43
Figure 35: Layout of 4x4 Ka-band array with Wilkinson dividers (RT/Duroid).	44
Figure 36: Simulated return loss and radiation pattern of Ka-band 4x4 array with Wilkinson dividers. (RT/Duroid).	44
Figure 37: Process for fabricating embedded resistor for Wilkinson power divider; (a) laminated resistor on LCP, (b) patterned Cu and resistor, (c) resistor with copper terminal pads.	49
Figure 38: Layout of Wilkinson divider with embedded resistor as fabricated.	49
Figure 39: Mask layout and fabricated antenna arrays.	50

Figure 40: Photos of front and back side of receive 8x8 array during radiation measurement.	51
Figure 41: NFR scan of 8x8 antenna array.	51
Figure 42: Measured return loss of (a) 4x1 and (b) 8x1 antenna arrays (ULTRALAM 3850).	52
Figure 43: Measured vs. simulated radiation patterns for 4x1 array (ULTRALAM 3850).	52
Figure 44: Measured vs. simulated radiation patterns for 8x1 array with integrated LNA (ULTRALAM 3850).	53
Figure 45: Measured vs. simulated return loss of 4x1 array with feed network using T-junctions (RT/Duroid® 5880LZ).	53
Figure 46: Measured vs. simulated radiation patterns for 4x1 array with T-junctions (RT/Duroid® 5880LZ).	54
Figure 47: Measured vs. simulated return loss of 8x2 array with feed network using T-junctions (RT/Duroid® 5880LZ).	54
Figure 48: Measured vs. simulated radiation patterns for 8x2 array with T-junctions (RT/Duroid® 5880LZ).	55
Figure 49: Measured vs. simulated return loss of 8x8 array with feed network using T-junctions (RT/Duroid® 5880LZ).	55
Figure 50: Measured vs. simulated radiation patterns for 8x8 array with T-junctions (RT/Duroid® 5880LZ).	55
Figure 51: Measured vs. simulated return loss for 4x1 array with Wilkinson dividers (RT/Duroid® 5880LZ).	56
Figure 52: Measured vs. simulated radiation patterns for 4x1 array with Wilkinson dividers (RT/Duroid® 5880LZ).	57
Figure 53: Measured vs. simulated return loss for 8x8 array with Wilkinson dividers (RT/Duroid® 5880LZ).	57
Figure 54: Measured vs. simulated normalized radiation patterns for 8x8 array with Wilkinson dividers (RT/Duroid® 5880LZ).	57
Figure 55: Measured radiation patterns for 8x8 array with T-junctions at different phase shift values.	58

## SUMMARY

Array antennas are used extensively in remote sensing applications, where a highly directive beam is needed to scan a particular area of interest on the surface of the earth. The research presented here focuses on the design of different microstrip patch antenna arrays to be used in environmental sensing applications in the X and Ka frequency bands, such as measurements in Snow and Cold Land Processes (SCLP) to detect snow accumulation, snow melt, etc. The goal of this research is to produce highly integrated, low loss, and compact size antenna arrays, while maintaining low power consumption. Multilayer organic (MLO) System-on-a-Package (SOP) technology, using laminates such as Liquid Crystal Polymer (LCP) and RT/Duroid®, provides a lightweight and low cost 3D solution for the fabrication of the antenna arrays.

The elements of the antenna arrays are rectangular patches. Two feeding mechanisms, aperture coupling and via feed, were implemented and compared. For the RF distribution network and interconnects, a corporate feed approach was used with reactive T-junctions, Wilkinson dividers, or both, for power division. The feed networks were designed using microstrip. The basic multilayer antenna array design consists of 3 layers of cladded laminate material. The metal layers are as follows: 1) patch antennas, 2) ground plane, 3) feed network, and 4) surface-mount components. The surface mount components would include LNA, PA, TR switch and phase shifter.

# CHAPTER 1

## INTRODUCTION

### 1.1 Overview of Antennas

An antenna is the transitional structure between free space and a guiding device, or transmission line. The transmission line is used to transport the electromagnetic energy from the transmitting source to the antenna or from the antenna to the receiver. In an ideal transmitting system, the antenna should radiate all the energy generated by the source. However, in a practical system there are conduction losses due to the lossy nature of the transmission line and the antenna, as well as due to reflection (mismatch) losses at the interface between the line and the antenna. Antennas must be properly designed to avoid reflected waves from the interface, which create interference (standing waves) inside the transmission line. Losses due to the line, antenna, and standing waves are undesirable. Choosing low loss materials can minimize the losses due to the line and antenna. The standing waves can be reduced by matching the impedance of the antenna to the characteristic impedance of the line. [1]

In addition to receiving or transmitting, an antenna is usually required to accentuate the radiating energy in some directions and suppress it in others. The antenna is one of the most critical components of a wireless system. A good antenna design can relax system requirements and improve overall system performance. Antenna technology has been around for many decades, but new applications and demand for greater system performance are constantly arising, and innovative antenna designs remain a challenge. New applications include high accuracy airborne navigation, global weather, and earth resource systems. Because of the many applications, the lower portion of the EM spectrum has been saturated, and the designs have been pushed to higher frequencies. [1]

Many applications require radiation characteristics that may not be achievable by

a single element, so an aggregate of radiating elements in an electrical and geometrical arrangement (an array) is often used. The arrangement of the array may be such that the radiation from the elements adds up to give a radiation maximum in a particular direction, and minimum in others. Arrays are the most versatile antenna systems. They find many applications in space-borne as well as earthbound missions. In most cases the elements of an array are identical, which is simpler and more practical. The main lobe can be scanned by controlling the relative phase excitation between the elements. The beam-width of the main lobe as well as the side lobe level can be controlled by the relative amplitude excitation of the array elements. [1]

## 1.2 Fundamental Parameters of Antennas

Some parameter definitions necessary to describe the performance of an antenna are given below. [2]

- *Radiation Pattern*: Mathematical function or graphical representation of the radiation properties of the antenna as a function of space coordinates. In most cases the radiation pattern is determined in the far-field region. The radiation property of most concern is the spatial distribution of radiated energy.
- *Directivity*: Ratio of radiation intensity in a given direction from the antenna to the radiation intensity averaged over all directions. If the direction is not specified, the direction of maximum intensity is implied. (Dimensionless)
- *Gain*: The relative gain is the ratio of the power gain in a given direction to the power gain of a reference antenna in its referenced direction. In most cases the reference antenna is a lossless isotropic source. When the direction is not stated, the power gain is usually taken in the direction of maximum radiation. (Dimensionless)
- *Efficiency*: Antenna radiation efficiency is the ratio of the power radiated to the input power. It relates the gain and directivity. Radiation efficiency takes into account conduction and dielectric losses. (Dimensionless)

- *Bandwidth:* Range of frequencies within which the performance of the antenna conforms to a specified standard. For narrowband antennas, the bandwidth is expressed as a percentage of the frequency difference (upper minus lower) over the center frequency. When the impedance is the limiting factor, the bandwidth is characterized in terms of the Q.

- *Polarization:* The polarization of an antenna in a given direction is the polarization of the wave transmitted (radiated) by the antenna. When the direction is not stated, the polarization is taken to be the polarization in the direction of maximum gain. Polarization describes the time varying direction and relative magnitude of the E-field.

- *Input Impedance:* Impedance presented by an antenna at its terminals, or ratio of the voltage and current at a pair of terminals, or ratio of the appropriate components of the electric and magnetic field at a point.

### **1.3 The Research Presented**

Array antennas are used extensively in remote sensing applications, where a highly directive beam is needed to scan a particular area of interest on the surface of the earth [3]. This research study focuses on the design of different microstrip patch antenna arrays to be used in environmental sensing applications in the X and Ka frequency bands, such as measurements in Snow and Cold Land Processes (SCLP) to detect snow accumulation, snow melt, etc. The goal of this research is to produce highly integrated, low loss, and compact size antenna arrays. Multilayer organic (MLO) System-on-a-Package (SOP) technology, using Rogers' ULTRALAM 3850 (LCP) and RT/Duroid® 5880LZ laminates, provides a lightweight and low cost 3D solution for the fabrication of the antenna arrays. SOP has provided a prominent solution for high-level integration of radio frequency (RF) front-end modules, which efficiently combines the up-to-date system-on-chip (SOC) solution with passive integration technologies such as MLO [4].

The antenna elements used for the arrays are rectangular microstrip patches. Two feeding mechanisms, aperture coupling and via feed, were implemented and compared. For the RF distribution networks and interconnects, a corporate feed approach was used with reactive T-junctions, Wilkinson dividers, or both, for power division. The feed networks were designed using microstrip. The basic multilayer antenna array design consists of 3 layers of cladded laminate material. The metal layers are as follows: 1) patch antennas, 2) ground plane, 3) y-direction feed network, and 4) x-direction feed network and surface-mount components. The surface mount components would include a LNA, PA, TR switch, and phase shifter. Different design variations can be pursued based on the needs of the desired application. An important part of this research was determining how to best avoid cross coupling between the feed network on the 3d metal layer and the RF electronics on the 4th metal layer, while still achieving a compact design. With this purpose, different layout options were investigated.

## CHAPTER 2

### BACKGROUND

Microstrip antennas became very popular in the 1970s primarily for space-born applications. Today they are used for both government and commercial applications. Microstrip antennas are low-profile, light-weight, conformable to planar and non-planar surfaces, simple and inexpensive to fabricate using modern printed-circuit technology, mechanically robust when mounted on rigid surfaces, compatible with Monolithic Microwave Integrated Circuits (MMICs), and versatile in terms of resonant frequency, polarization, pattern, and impedance. Disadvantages of microstrip antennas include their low efficiency, low power, and limited bandwidth (1-5%); although larger bandwidths can be achieved with increased complexity. Microstrip antennas can be mounted on the surface of aircraft, spacecraft, satellites, missiles, ground vehicles, handheld wireless communications devices, etc. [1]

Microstrip antennas consist of a metallic patch on a grounded dielectric substrate; they are also referred to as *patch* antennas. The radiating elements and feed lines are usually photo-etched on the dielectric substrate. The metallic patch thickness is  $t \ll \lambda_0$  (where  $\lambda_0$  is the free space wavelength) and the substrate height is  $h \ll \lambda_0$ , usually  $0.003\lambda_0 \leq h \ll 0.05\lambda_0$ . The metallic patch can take many different configurations, the most common of which is a rectangular patch as seen in Figure 1. This configuration is the most popular because of ease of analysis and fabrication, and its radiation characteristics, especially low cross-polarization radiation. [1]

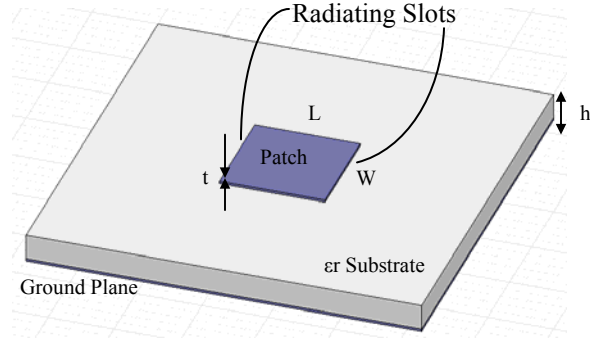


**Figure 1.** Microstrip antenna.

The quality factor, bandwidth, and efficiency, are antenna figures-of-merit that are interrelated, so there is always a tradeoff when optimizing the antenna's performance. Thick substrates with a low dielectric constant provide better efficiency, larger bandwidth, and loosely bound fields for radiation into space, but at the expense of element size. Furthermore, as the substrate height increases, surface waves may be introduced, which usually are not desirable because they extract power from the total available for direct radiation (space waves). Surface waves travel within the substrate and are scattered at bends and surface discontinuities, such as the boundary of the dielectric and ground plane, and degrade the antenna pattern and polarization characteristics. [1]

The quality factor is representative of the antenna losses. There are radiation, conduction (ohmic), dielectric, and surface wave losses that affect the total quality factor, which is written as

$$\frac{1}{Q_t} = \frac{1}{Q_{rad}} + \frac{1}{Q_c} + \frac{1}{Q_d} + \frac{1}{Q_{sw}}. \quad (1)$$

For very thin substrates ( $h \ll \lambda_0$ ) the losses due to surface waves are very small and can be neglected. For very thin substrates of arbitrary shapes, the approximate formulas to represent the quality factors associated with the various losses are as follows:

$$Q_c = h\sqrt{\pi f \mu \sigma} \quad (2)$$

$$Q_d = \frac{1}{\tan \delta} \quad (3)$$

$$Q_{rad} = \frac{2\omega\epsilon_r}{hG_t/l} K \quad (4)$$

where  $\epsilon_r$  is the substrate dielectric constant and  $G_t/l$  is the total conductance per unit length, and

$$K = \frac{\iint_{area} |E|^2 dA}{\oint_{perimeter} |E|^2 dl} \quad (5)$$

Since  $Q_{rad}$  is inversely proportional to the height of the substrate, it is usually the dominant factor. [1]

The fractional bandwidth of the antenna is inversely proportional to  $Q_t$ , and is defined by

$$\frac{\Delta f}{f_0} = \frac{VSWR - 1}{Q_t \sqrt{VSWR}} \quad (6)$$

The VSWR at the input is equal to or less than a desired value over a band of frequencies, assuming that the VSWR is unity at the design frequency. The bandwidth is proportional to the volume of the microstrip antenna. The radiation efficiency is defined as the power radiated over the input power; it can also be expressed in terms of the quality factors as

$$e_{cdsw} = \frac{1/Q_{rad}}{1/Q_t} = \frac{Q_t}{Q_{rad}} \quad (7)$$

The pattern of the microstrip antenna has its maximum normal to the patch (broadside radiator). This is accomplished by properly choosing the field configuration beneath the patch. [1] The lowest order mode  $TM_{10}$  (anti-symmetric voltage distribution), resonates when the effective length across the patch is a half-wavelength [5]. The size of the patch is inversely proportional to the frequency of operation of the antenna, and dependent on the effective dielectric constant  $\epsilon_{eff}$  of the microstrip. The

effective dielectric constant of a microstrip structure satisfies the relation  $1 < \epsilon_{\text{eff}} < \epsilon_r$ , since some of the field lines are in the dielectric region and some are in the air. The effective dielectric constant is dependent on substrate thickness  $t$  and conductor width  $W$  as follows [6]:

$$\epsilon_{\text{eff}} = \frac{\epsilon_r + 1}{2} + \frac{\epsilon_r - 1}{2} \left( 1 + 12 \frac{h}{W} \right)^{-1/2} \quad (8)$$

## 2.1 Microstrip Antenna Modeling

The most popular methods of analysis for microstrip antennas are the *transmission-line*, *cavity*, and *full-wave*. The transmission line model gives good physical insight, but it is less accurate. The cavity model also gives good physical insight and is more accurate than the transmission-line model, but it is more complex. The full-wave model is very accurate and versatile, and it can model coupling, which is difficult to do with the first two methods; however, it usually gives less physical insight and is the most complex model. [1]

The rectangular patch is by far the most widely used configuration of a microstrip antenna. A rectangular patch is simple enough to be modeled with the transmission-line model, which represents the antenna by two slots, separated by a low-impedance transmission line of length  $L$ . [1] These two slots are the radiating edges of the patch, which are loaded with a combination of parallel-plate radiation conductance and capacitive susceptance [4]. Each radiating slot is thus represented by a parallel equivalent admittance  $Y = G + jB$ , where  $G$  is the conductance and  $B$  the susceptance. This is shown in Figure 2 with the slots labeled 1 and 2. Since slot 1 is identical to slot 2, the equivalent admittance is  $Y_1 = Y_2$ ,  $G_1 = G_2$ ,  $B_1 = B_2$ . [1] The conductance is given by

$$G = \frac{W}{120\lambda_0} \left[ 1 - \frac{1}{24} (k_0 * h)^2 \right] \quad \frac{h}{\lambda_0} < \frac{1}{10} \quad (9)$$

Where  $k_0 = 2\pi/\lambda_0$  and  $\lambda_0$  is the free-space wavelength.

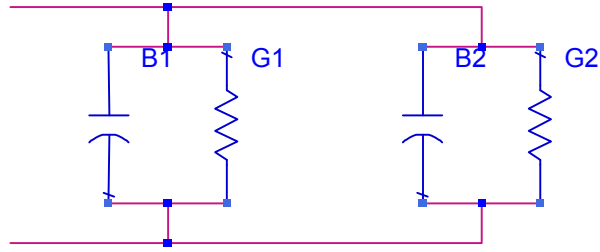


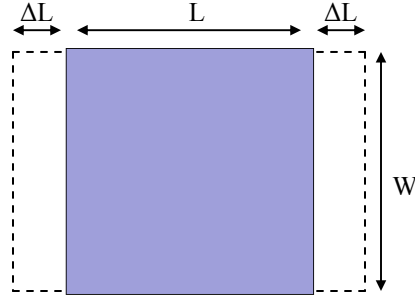
**Figure 2.** Transmission model equivalent of microstrip patch.

The width of the transmission line determines the impedance and effective dielectric constant, and is given by

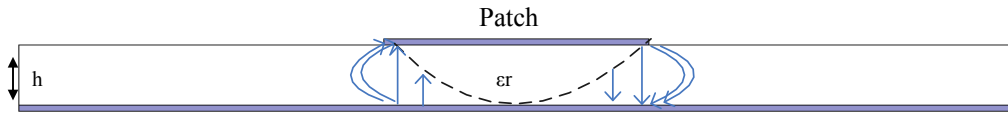
$$W = \frac{v_0}{2f_r} \sqrt{\frac{2}{\epsilon_r + 1}} \quad (10)$$

where  $v_0$  is the free-space velocity of light, and  $f_r$  is the resonant frequency. The length  $L$  is usually  $\lambda_0/3 < L < \lambda_0/2$ . The fields at the four edges of the patch undergo fringing, which makes the patch look larger electrically compared to its physical dimensions. The use of an effective dielectric constant  $\epsilon_{eff}$  accounts for fringing and the wave propagation in the line. Figure 3 shows the effect of fringing on the electrical length of the patch. The length is extended on each end by a distance  $\Delta L$ . The normalized extension of the length is approximated by

$$\frac{\Delta L}{h} = 0.412 \frac{(\epsilon_{reff} + 0.3) \left( \frac{W}{h} + 0.264 \right)}{(\epsilon_{reff} - 0.258) \left( \frac{W}{h} + 0.8 \right)}. \quad (11)$$



(a) Top view



(b) Side view

**Figure 3.** Fringing effect on length of patch.

The effective length of the patch then becomes  $L_{eff} = L + 2\Delta L$ , where  $L = \lambda/2$  for dominant  $TM_{10}$  mode without fringing [1]. Here  $\lambda = \lambda_0/\sqrt{\epsilon_{reff}}$  is the wavelength in the dielectric. For the dominant  $TM_{10}$  mode, the resonant frequency of the microstrip antenna including edge effects is given by

$$fr_{10} = \frac{v_0}{2(L + 2\Delta L)\sqrt{\epsilon_{reff}}}. \quad (12)$$

Solving this equation for the actual length of the patch gives  $L = \lambda/2 - 2\Delta L$ , or

$$L = \frac{v_0}{2f_r\sqrt{\epsilon_{reff}}} - 2\Delta L; \quad (13)$$

therefore  $L$ , which represents the separation of the slots, is slightly less than  $\lambda/2$ ; typically  $0.48\lambda < L < 0.49\lambda$  [1].

The bandwidth of a rectangular microstrip antenna at a constant resonant frequency can be expressed as

$$BW \sim volume = length * width * height \sim \frac{1}{\sqrt{\epsilon_r}} \frac{1}{\sqrt{\epsilon_r}} \sqrt{\epsilon_r} = \frac{1}{\sqrt{\epsilon_r}}, \quad (14)$$

therefore the bandwidth is inversely proportional to the square root of the dielectric constant of the substrate. The directivity of a rectangular patch antenna (two slots) when  $k_0 \cdot h \ll 1$  can be written as

$$D_2 = \left( \frac{2\pi W}{\lambda_0} \right)^2 \frac{\pi}{I_2}; \quad (15)$$

Asymptotically the directivity can be expressed as

$$D_2 = \begin{cases} 6.6 = 8.2 \text{ dB} & W \ll \lambda_0 \\ 8 \left( \frac{W}{\lambda_0} \right) & W \gg \lambda_0 \end{cases} \quad (16)$$

## 2.2 Feeding Methods

There are many configurations that can be used to feed microstrip antennas. The most popular ones are microstrip line, aperture coupling, and via. The microstrip line is a  $50\text{-}\Omega$  line attached to the center of one of the radiating edges; this approach is not desirable since the line would become very wide on the low dielectric constant substrate containing the radiating patch. The two latter configurations are described below.

### 2.2.1 Aperture Coupling Feed

Aperture-coupled microstrip antennas typically have a narrow bandwidth, and are difficult to fabricate. However, they are somewhat easy to model and have moderate spurious radiation. Figure 4 shows an aperture coupling feed and its equivalent circuit. The aperture coupling consists of two substrates separated by a ground plane. On the bottom side of the lower substrate there is a microstrip feed line whose energy is coupled to the patch through a slot on the ground plane between the two substrates. This arrangement allows independent optimization of the radiating element and the feed line.

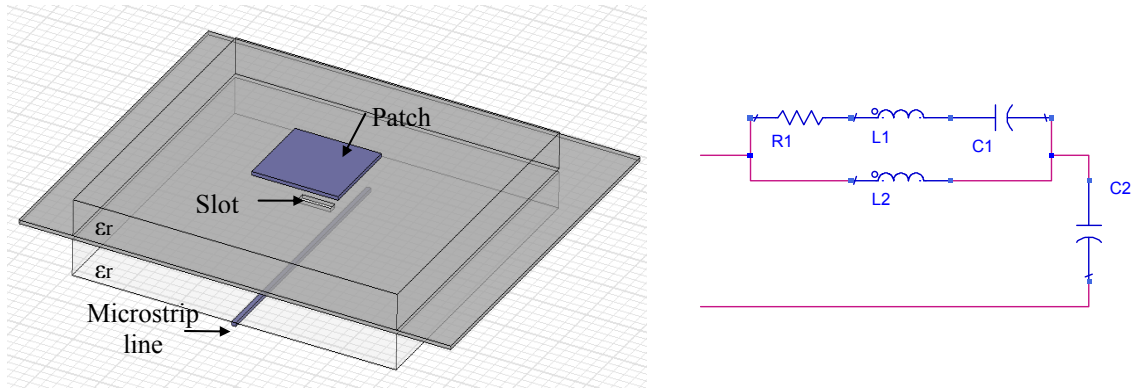


**Figure 4.** Aperture-coupled feed and its equivalent circuit.

The ground plane separating the substrates isolates the feed from the patch minimizing spurious radiation, which would interfere with pattern formation and polarization purity. The substrate parameters, feed line width, and slot size, are used to optimize the design. Coupling through the slot can be modeled through the theory of Bethe, in which the slot is modeled by an equivalent normal electric dipole to account for the normal component of the electric field, and an equivalent tangential magnetic dipole to account for the tangential component of the magnetic field. The magnetic coupling will dominate when the slot is centered below the patch, where ideally the electric field is zero and the magnetic field is at maximum. This will also contribute to good polarization purity and no cross-polarized radiation. [1]

### 2.2.2 Via Feed

Via-fed patches are easier to fabricate and match, and they have lower spurious radiation. However they also have a narrow bandwidth, and they are more difficult to model, especially in thick substrates ( $h > 0.02\lambda_0$ ). This type of feed configuration has inherent asymmetries, which generates higher order modes that produce cross-polarized radiation. [1] Figure 5 shows a via feed and its equivalent circuit.

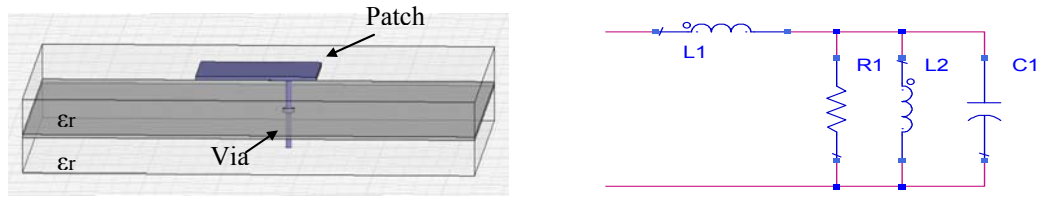


**Figure 5.** Via feed and its equivalent circuit.

The patch is fed along the resonant length. The radiating edge fields are expanded in an odd mode, since the power traveling across the patch loses  $180^\circ$  of phase (patch is approximately a half-wavelength long in the dielectric). The odd mode creates a virtual short circuit halfway through the patch. A shorting pin from the center of the patch to the ground layer has no effect on radiation or impedance, but it allows low frequency grounding of the antenna. The feed location does not affect the resonant frequency significantly, but it affects the input impedance as it varies from the center to the edges of the patch. The input conductance of the patch fed on the edge is twice the conductance of one of the edge slots. [5]

### 2.3 Microstrip Antenna Arrays

The radiation pattern of a single-element antenna is relatively wide, and the values of directivity (and gain) are relatively low. Applications such as remote sensing require a highly directive beam (and high gain), which can be accomplished by increasing the size of the antenna. As the electrical size of the antenna increases the beam becomes narrower, but the sidelobes become larger, which limits the directivity. A way of enlarging the dimensions of the antenna without necessarily increasing the size of an individual element is to form an array. Combining antennas into an array allows for improved control over the radiation pattern and better focus of the radiated energy. In most cases the elements of an array are identical. [1]

The total field of the array is given by the vector addition of the fields of individual elements. This assumes the current in each element is the same, which is

usually not the case and depends on the separation between elements. In an array of identical elements, controlling the following parameters can shape the overall pattern of the antenna:

- Geometrical configuration of array (linear, rectangular, etc.)
- Separation between elements
- Excitation amplitude of individual elements
- Excitation phase of individual elements
- Pattern of individual elements

In microstrip arrays, mutual coupling between elements is present; therefore full-wave solutions are required to obtain accurate results.

### 2.3.1 N-Element Uniform Linear Array

A uniform array is an array of identical elements fed with currents of equal magnitude and a linear progressive phase. A progressive phase means that the current of each succeeding element leads the current of the preceding element by a factor  $\alpha$ .

Assume that the elements of the array are oriented in the x-direction and positioned along the x-axis with a uniform spacing  $d$  as seen in Figure 6. The path length between the  $n$ -th element and a far-zone observer is given by

$$\rho_n \approx \rho_1 - (n-1) d \sin\theta. \quad (17)$$

The total electric field radiated, assuming no coupling between elements, is equal to the sum of the individual elements' fields. It has been shown that the far-zone field of a uniform array can be expressed as the field of a single element multiplied by a factor called the array factor. [1] That is,

$$E(\text{total}) = [E(\text{single element at reference point})] \times [\text{array factor}] \quad (18)$$

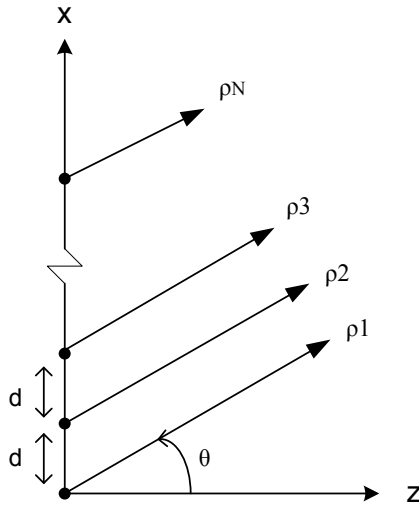


**Figure 6.** Far-field geometry of n-element array with elements uniformly spaced along the x-axis.

The array factor is a function of the number of elements, the geometry of the array, the excitation phase, and the spacing. By varying the phase  $\alpha$  between elements, the characteristics of the array factor and of the total field of the array can be controlled. Since the array factor does not depend on the directional characteristics of the radiating elements themselves, the elements can be replaced with isotropic (point) sources. The total field is then calculated multiplying the array factor of the isotropic sources by the field of a single element. This is referred to as pattern multiplication, and it applies only for arrays of identical elements. [1] The magnitude of the array factor is given by

$$|A(\theta)| = \left| \frac{\sin(N\psi/2)}{\sin(\psi/2)} \right| \quad (19)$$

where

$$\Psi = kd \sin \theta + \alpha \quad (20)$$

and  $d$  is expressed in terms of  $\lambda$ .

The array factor is maximum at the angle  $\theta$  that makes  $\Psi = 0$ . There is only one maximum (main lobe), but there are also secondary maxima (maxima of minor/grating lobes) that arise due to large element spacing. The large spacing provides other

directions in which the currents add in phase. Grating lobes are usually not desired, and can be controlled by constraining the distance between elements. The distance necessary to avoid grating lobes is given by

$$d = \frac{\lambda(N-1)}{N(\sin \theta_s + 1)} \quad (21)$$

where  $\theta_s$  is the scanning angle and  $\lambda$  is the maximum wavelength. Making the sidelobe level small, however, increases the beam-width of the main lobe; this tradeoff needs to be taken into account when designing the antenna array. A good design is essential, especially in applications such as remote sensing, in which highly directive antennas are desired, so the antenna arrays must exhibit both a narrow main beam and low sidelobes.

The maximum radiation (main lobe) can be directed in any direction  $\theta$  using a progressive phase shift  $\alpha$ , and thus forming a phased (scanning) array. In phased array technology the scanning should be continuous, so the system should be capable of continuously varying the phase between the elements. This can be accomplished electronically with the use of phase shifters.

### **2.3.2 Feed Networks**

Feed lines require thin substrates in order to have tightly bound fields to minimize undesired radiation and coupling, and to reduce the dimensions of the line. On the contrary, microstrip antennas require thick substrates for improved bandwidth [1]; therefore having the feed network on a separate layer improves the overall performance of the system since it allows for independent optimization of antenna elements and feed lines. The elements of an array can be fed by a single line, as shown in Figure 7(a); this is called a series feed network. They can also be fed by multiple lines, as shown in Figure 7(b); this is called corporate feed network. The research presented here makes use of corporate feed networks.

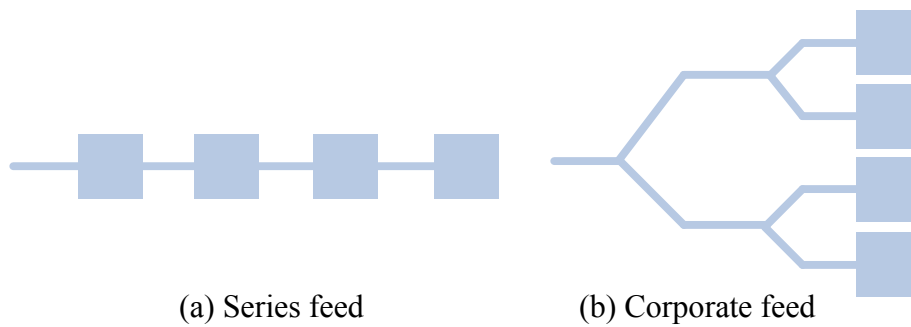


**Figure 7.** Feed network arrangements for microstrip patch arrays.

Corporate feed networks allow more control of the feed of each element (amplitude and phase); therefore they are ideal for scanning phased arrays, multi-beam arrays, or shaped-beam arrays [1]. The amplitude can be changed with either attenuators or amplifiers, while the phase can be controlled with phase shifters as mentioned in the previous section. Having a multilayer system prevents feed line radiation interference with the antenna performance, which would limit sidelobe levels and introduce cross-polarization. [7] The feed network can be connected to the antenna elements using feeding mechanisms such as aperture coupling and via feed, which were described in section 2.2. A corporate feed network provides power splits of  $2^n$ , for  $n = 2, 4, 6$ , etc. The power can be split using three-port power dividers of equal division (3 dB). An ideal power divider is lossless, reciprocal, and matched at all ports. However, it has been shown that such a network is impossible to construct. One of the three conditions must be relaxed for the device to be physically realizable. [6] Two types of power dividers are described below.

#### 2.3.2.1 T-Junction Power Divider

T-junctions are reciprocal and can be considered lossless if transmission line loss is not taken into account. Thus, as discussed above, they cannot be matched at all ports. A lossless T-junction can be modeled as a junction of three transmission lines, as shown

in Figure 8. For the divider to be matched to the input line of characteristic impedance  $Z_0$ , the following must be true:

$$\frac{1}{Z_1} + \frac{1}{Z_2} = \frac{1}{Z_0}. \quad (22)$$

For an equal split power divider with  $Z_0 = 50 \Omega$ ,  $Z_1$  and  $Z_2$  would be  $100\Omega$ . Quarter wave transformers can be used to bring the output line impedances back to the characteristic impedance  $Z_0$ . There is no isolation between the output ports. [6]

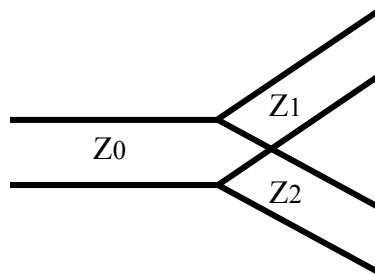


**Figure 8.** Transmission Line Model of a lossless T-junction.

A quarter-wave transformer matches the input and output impedances of a system by placing a lossless,  $\lambda/4$ -long transmission line of characteristic impedance  $Z_{qw}$ , between the input and output lines. Figure 9 shows a circuit employing a quarter-wave transformer in which both the feed line and the load characteristic impedances,  $Z_c$  and  $Z_L$  respectively, are known and real. In order to match the load to the feed line, the input impedance  $Z_{in}$  looking into the quarter-wave matching section must be equal to  $Z_c$ . This is achieved when

$$Z_{qw} = \sqrt{Z_c Z_L}. \quad (23)$$

This condition applies only when the length of the matching section is  $\lambda/4$ -long or an odd multiple of it  $((2n+1)*(\lambda/4))$ , for a perfect match at a single frequency. Mismatch would occur at other frequencies. [6]

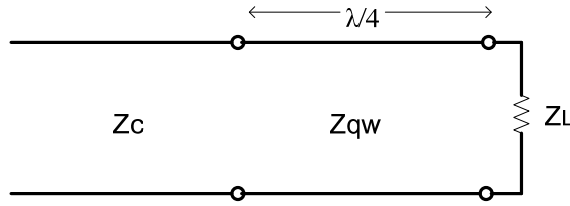


**Figure 9.** Quarter-wave matching transformer.

### 2.3.2.2 Wilkinson Power Divider

The lossless T-junction is not matched at all ports (unless quarter-wave transformers are used), and it has no isolation between output ports. The Wilkinson divider is an alternative reciprocal three-port matching network that can be made having all ports matched and the output ports isolated from each other. However, the Wilkinson divider is not lossless, since reflected power is dissipated using a resistor. The transmission line circuit of an equal-split (3 dB) Wilkinson divider is shown in Figure 10.

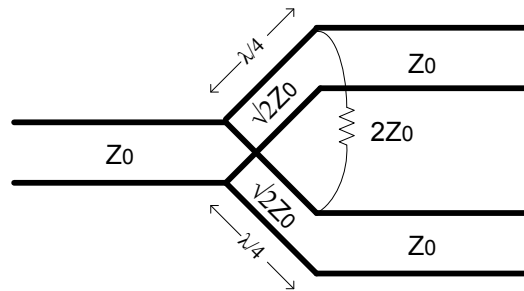


**Figure 10.** Equivalent transmission line circuit of equal-split Wilkinson power divider.

The values for the impedance of the quarter-wave lines and the resistor connecting the output ports are given by an even-odd mode analysis. [6] When ports 2 and 3 are terminated in matched loads, the input impedance at port one is

$$Z_{in} = \frac{1}{2}(\sqrt{2})^2 = 1. \quad (24)$$

No power is dissipated in the resistor when the divider is driven at port one and the outputs are matched; only reflected power from ports 2 or 3 is dissipated in the resistor.

Reflected signals don't propagate to other paths in the system, so the output ports are isolated.

## **CHAPTER 3**

### **DESIGN AND SIMULATION OF ANTENNA ARRAYS**

The design and simulation of multilayer microstrip antenna arrays intended for environmental sensing applications is described in this chapter. Microstrip antennas are advantageous for their low cost to fabricate, ease to form a large array, and light weight. The patch antennas used for the arrays are rectangular, and they are fed using either aperture coupling or via feed. A corporate feed network approach is used for the power distribution of the antenna arrays, and T-junctions or Wilkinson power dividers are used in the designs. The substrate materials used to implement the microstrip antennas are ULTRALAM, a material using liquid crystalline polymer (LCP) as the dielectric film, [8] and RT/Duroid [9]. These materials are flexible, lightweight, durable, and resistant to radiation, which make them ideal for radar applications [10]. The size of the radiating elements depends on the dielectric constant of the film, and the desired frequency of operation. Most of the arrays were designed at X-band, for which the size of each patch is on the order of 1 cm. The last array presented was designed at Ka-band, and it's on the order of .3 cm.

#### **3.1 Substrate Material**

The choice of substrate is very important for the performance of any RF system. For low frequency analog and digital systems most PCB manufacturers use woven glass and epoxy-based materials, such as FR-4. However, for high frequency applications, the dielectric material adds significant loss, so these types of materials are not suitable. [11] The substrates that are most desirable for good antenna performance are thick substrates with low dielectric constants because they provide better efficiency, larger bandwidth, and loosely bound fields for radiation into space. Feed networks require tightly bound

fields to minimize undesired radiation and coupling; therefore thin substrates are desirable. Thin substrates also lead to smaller element sizes. The chosen substrate material should have constant dielectric control, low dissipation factor, and controlled thickness [12]. The substrate should allow for low cost fabrication and multilayer integration as well as easy integration with embedded resistors and surface-mount active components. Furthermore, it should be lightweight, mechanically robust, and allow for conformity to planar and non-planar surfaces. The flexibility of the material is very important for antennas in remote sensing applications since they have to conform, for instance, to the shape of an airplane surface where they are mounted. Two materials provided by Rogers Corporation were used in this research. They are ULTRALAM 3850 Liquid Crystalline Polymer Circuit Material [8] and RT/Duroid® 5880LZ High Frequency Laminate [9].

### **3.1.1 ULTRALAM 3850 Laminate**

This adhesive-less laminate utilizes high temperature resistant LCP as the dielectric film, and it's suitable for multilayer constructions. LCP is ideal for RF packaging and multilayer integration because when melted into its liquid crystal state, it forms strong bonds with other LCP layers, creating a single uniform dielectric [3]. ULTRALAM 3850 is offered as a double copper clad laminate, and it's used in high frequency and high performance applications. Satellites and radars are some of the typical applications of this substrate material. For multilayer constructions, it can be used with ULTRALAM 3908 bonding film. LCP has a low and stable dielectric constant and dielectric loss; Appendix A shows the comparison between LCP and other types of laminates. ULTRALAM 3850 is compatible with standard PCB fabrication. Some of its features are:

*Excellent high frequency properties*

- Stable electrical properties for controlled impedance matching

- Thickness uniformity for signal integrity
- Thinner dielectric layer with minimal signal distortion

*Dimensional Stability*

- Low modulus: Bends easily for conformity, offers design flexibility, maximizes circuit density
- Low moisture absorption: Reduces bake times, maintains stable properties in humid environments
- Flame resistant: Halogen-free

Table 1 shows some of the properties of ULTRALAM 3850 [8].

**Table 1:** Properties of ULTRALAM 3850 Laminate

<b>Properties</b>	<b>Value</b>
Dielectric Constant $\epsilon_r$ , 10 GHz, 23°C	2.9
Dissipation Factor $\tan \delta$ , 10 GHz, 23°C	.0025
Standard Thickness	0.001" (25 $\mu\text{m}$ )
	0.002" (50 $\mu\text{m}$ )
	0.004" (100 $\mu\text{m}$ )
Standard Copper Cladding	½ oz. (18 $\mu\text{m}$ )

**3.1.2 RT/Duroid® 5880LZ Laminate**

RT/Duroid® 5880LZ is a copper-clad filled PTFE composite used in demanding stripline and microstrip circuit applications. The filler is low density and lightweight; suitable for high performance, weight sensitive applications. The very low dielectric constant of this laminate is uniform from panel to panel and constant over a wide frequency range; the dissipation factor is also very low. RT/Duroid 5880LZ allows for easy circuit fabrication using standard PCB processes. Some of its features are:

- Lowest dielectric constant available
- Low Z-axis CTE
- Lightweight / low density

- Uniform electrical properties over frequency
- Lead-free process compatible

Table 2 shows some of the properties of RT/Duroid® 5880LZ [9].

**Table 2:** Properties of RT/Duroid® 5880LZ Laminate

Properties	Value
Dielectric Constant $\epsilon_r$ , 10 GHz, 23°C	1.96 ± 0.04
Dissipation Factor Tan $\delta$ , 10 GHz, 23°C	Typ.: .0019 Max.: 0.0027
Standard Thickness	0.010" (.254 mm) 0.020" (0.508 mm) 0.030" (0.762 mm) 0.060" (1.524 mm) 0.100" (2.540 mm)
Standard Copper Cladding	½ oz. (17 µm) 1 oz. (35 µm) 2 oz. (70 µm)

### 3.2 Antenna Arrays with Corporate Feed Networks using T-Junctions

Linear and planar antenna arrays of different sizes were designed with microstrip line feed networks employing reactive T-junctions. Figure 11 shows a cross-sectional view of the basic substrate stack-up used to implement the antennas. The top substrate layer is either ULTRALAM 3850 or RT/Duroid® 5880 LZ. The initial goal was to create the arrays using only the LCP-based ULTRALAM, taking full advantage of its superior bending capabilities. A few designs were completed in X-band using ULTRALAM 3850 for all three layers seen in Figure 11, using a dielectric thickness of 51 mils for the radiating patches layer (top layer). This thickness was chosen, after experimenting with different values, in order to achieve at least a 5% 10dB bandwidth for the antennas. The results obtained with these designs are presented here. Unfortunately, the ULTRALAM 3850 laminate became unavailable in the 50-mil thickness, so a

decision was made to replace the thick top substrate with RT/Duroid® 5880 LZ, while keeping the 4-mil and 3-mil layers ULTRALAM 3850. The dielectric thicknesses in Figure 11 include the necessary 1-mil bonding films to achieve the multilayer construction [8].

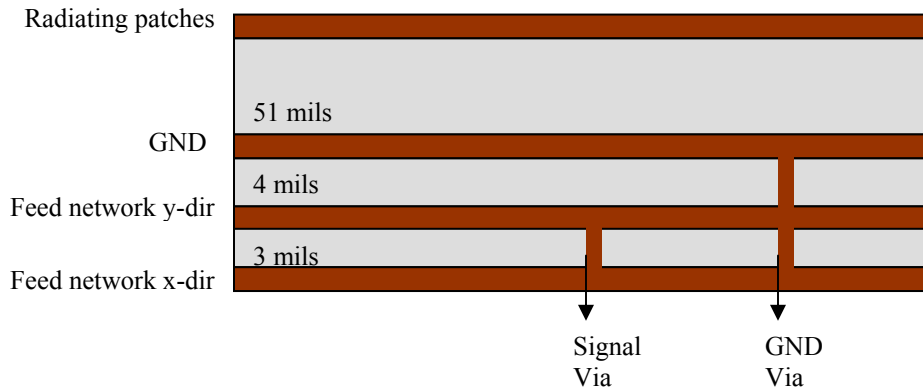


**Figure 11.** Cross-sectional view of substrate stack-up for X-band antenna arrays.

Two feed networks are used; one embedded connecting the patches in the y-direction, and another one on the bottom metal layer connecting the patches in the x-direction in the case of the planar arrays. The two feed networks are connected to each other through vias. Two separate layers are used for the feed networks to minimize cross coupling between the feed lines while still achieving a compact design, i.e. by separating the feed lines in the thickness direction ( $z$ ) the distances in the  $x$  and  $y$  directions can be reduced. In addition, having one of the feed networks embedded reduces the possibility of interference with active surface-mount components such as phase shifters, TR modules, LNAs, and PAs, that would be wire-bonded to a CBCPW line on the bottom metal layer. The power and control lines necessary for these components would also be printed on the bottom metal layer, so having at least part of the RF feed network on a different substrate layer provides a great advantage in terms of real state as well as signal integrity. To avoid cross coupling between lines on the same layer, a spacing of at least 3

times the width of the line, was used. Although the two feed networks are separated by a 3-mil substrate, there may still be some cross coupling between them; therefore the horizontal distances between lines in different layers were also carefully chosen. Simulations were performed to find the optimal spacing between lines on the same layers and different layers to avoid cross coupling and still achieve a compact design

Each reactive T-junction used in the antenna feed network provides an equal or 3dB power split. Figure 12 shows the layout of a T-junction used in the antenna feed network. The impedance of the input line is the characteristic impedance of the system ( $Z_0 = 50\Omega$ ), so the impedance of the output lines should be  $100\Omega$  as explained in section 2.3.2.1. However, the desired output impedance is also  $50\Omega$ , so quarter-wave transformers are used to bring the  $100\Omega$  impedances back to the characteristic impedance as shown in Figure 12. The width of the lines is inversely proportional to their impedance, and calculated using the microstrip line equations below, where  $d$  is the distance from the lines to the ground plane. [6]

$$\frac{W}{d} = \frac{8e^A}{e^{2A} - 2} \quad \text{for } W/d < 2$$

$$\frac{W}{d} = \frac{2}{\pi} \left[ B - 1 - \ln(2B - 1) + \frac{\epsilon_r - 1}{2\epsilon_r} \left\{ \ln(B - 1) + 0.39 - \frac{0.61}{\epsilon_r} \right\} \right] \quad \text{for } W/d > 2 \quad (25)$$

where

$$A = \frac{Z_0}{60} \sqrt{\frac{\epsilon_r + 1}{2}} + \frac{\epsilon_r - 1}{\epsilon_r + 1} + \left( 0.23 + \frac{0.11}{\epsilon_r} \right)$$

$$B = \frac{377\pi}{2Z_0\sqrt{\epsilon_r}}$$

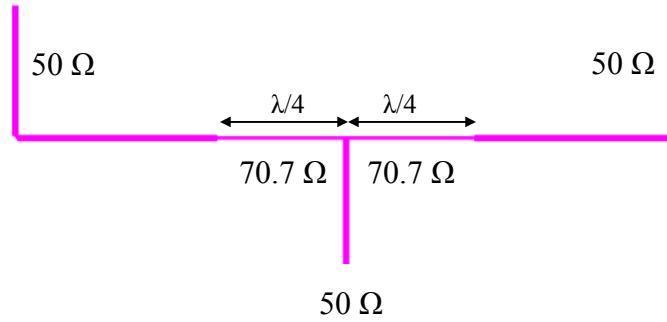


**Figure 12.** Layout of reactive T-junction used in RF feed networks.

The antenna arrays were designed with a center frequency of 9.5 GHz with a desired 10dB bandwidth of 500 MHz. They use one of two feeding mechanisms: aperture coupling or via-feed. The embedded feed network using T-junctions was designed and optimized, and linear arrays were created with elements positioned along the y-direction. Adjustments to parameters such as the patch length are usually needed when the single elements are integrated into an array, in order to obtain the desired performance characteristics, such as a certain return loss at the center frequency. Once the linear arrays are designed, they are used as building blocks to create planar arrays, with a feed network in the using T-junctions realized on the bottom metal layer of the substrate. The arrays designed are intended to be used in a phased array for a radar that scans in the x-direction only. Therefore, the phase of the elements must vary only in the x-direction, and stay constant in the y-direction. Thus the distance between elements in the y-direction was found with equation (21) with a maximum frequency of 9.75 GHz and a scan angle  $\theta_s = 0$ ; a distance of 27 mm was chosen. The distance between the elements in the x-direction was found using a desired scan angle  $\theta_s = 20^\circ$ ; a distance of 20 mm was chosen.

### 3.2.1 Aperture-Coupled Antenna Arrays

The antenna arrays were designed starting with a single element using the transmission line model described in Section 2.1. The single element antenna is a

rectangular patch fed by aperture coupling (see Section 2.2.1). A slot is opened in the ground plane centered below the patch, and the feed line is in the embedded metal layer below the ground plane. The microstrip feed line width was independently optimized using Agilent/ADS and Momentum. The size of the slot was calculated using the following equations:

$$L_{\text{slot}} = W_{\text{line}} + n * H_f \quad (26)$$

$$W_{\text{slot}} = (1/10) * L_{\text{slot}}$$

where  $W_{\text{line}}$  is the width of the microstrip feed line,  $H_f$  is the thickness of the substrate feed line, and  $n > 6$ . [13] The length of the open circuit stub from the slot is initially set to  $\lambda/4$ . The complete antenna was simulated and optimized using Agilent Momentum by adjusting the parameters: feed line width, antenna and slot dimensions, and length of open circuit stub.

#### 3.2.1.1 Antenna Arrays using ULTRALAM 3850

Design layouts and simulation results for antenna arrays of different sizes using ULTRALAM 3850 for all the substrate layers are shown here. Figure 13 shows a 4x1 array. The four different metal layers (patches, GND-slots, y-direction feed network, and bottom layer CBCPW) are shown in different colors. The signal via goes from the feed network to the bottom layer, and ground vias go from the grounds of the CPW line to the embedded ground plane. The CPW is intended to be used for the integration of the surface-mount active components that will complete the antenna system. The return loss and H-plane radiation pattern of the 4x1 array were simulated using Agilent Momentum; results are shown in figure 14. The 4x1 array was then used to create an 8x1 array. The layout and simulation results for the 8x1 array are shown in Figures 15 and 16. The dimensions for the 8x1 antenna array are summarized in table 3. The simulation results of both arrays are listed in Table 5.

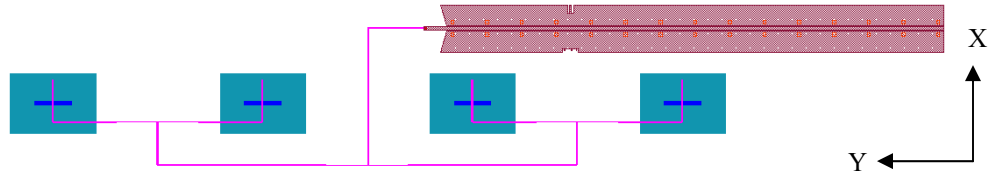


**Figure 13.** Layout of 4x1 array with aperture coupling and T-junctions (ULTRALAM).

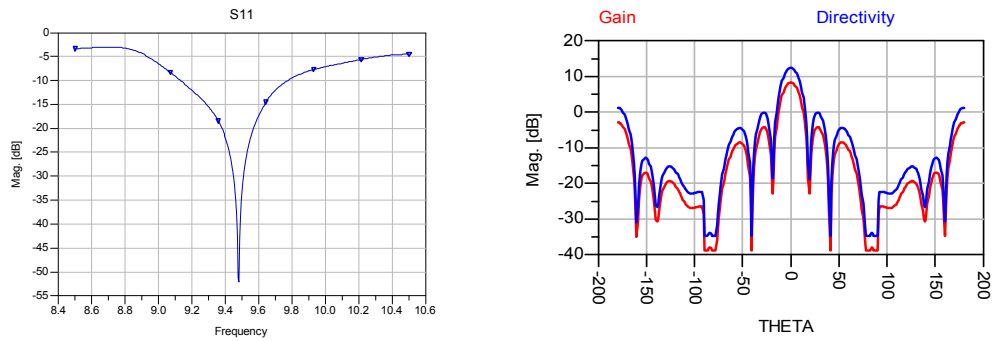


**Figure 14.** Simulated return loss and radiation pattern of 4x1 array with aperture coupling and T-junctions.

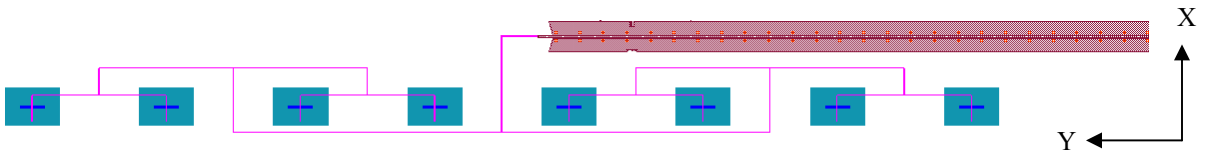


**Figure 15.** Layout of 8x1 array with aperture coupling and T-junctions (ULTRALAM).

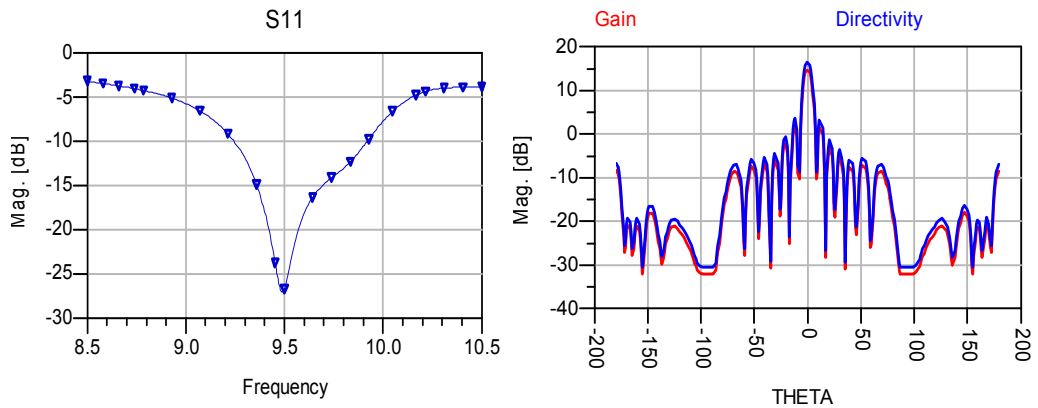


**Figure 16.** Simulated return loss and radiation pattern of 8x1 array with aperture coupling and T-junctions (ULTRALAM).

**Table 3:** Dimensions for 8x1 Array with T-Junctions using ULTRALAM 3850

Parameter	Value (mm)
50-Ω line width	.254
70-Ω line width	.138
Patch width	11.1
Patch length	7.71
Slot width	.501
Slot length	5
Open circuit stub length	2.64

**Table 4:** Simulation Results for Arrays with Aperture Coupling and T-Junctions using ULTRALAM 3850

	4x1 Array	8x1 Array
10dB Bandwidth (MHz)	643	677
Power Gain (dBi)	8.22	14.94

### 3.2.1.2 Antenna Arrays using RT/Duroid® 5880LZ

Antenna Arrays of different sizes were also designed using RT/Duroid® 5880LZ for the radiating patches substrate (top layer). Figures 17 through 22 show the layout and Momentum simulation results for a 4x1, an 8x2, and an 8x8 antenna array. Notice that, unlike the array designs shown in the previous section, these have a much shorter CPW line. The length of the CPW is just enough to fit the active surface-mount components, and CPW to microstrip transitions are used on both sides of the line. The CPW needed for an SMA connector is also included. The decision to shorten the CPW line was made after simulation results showed that this approach was less lossy. The dimensions for the 8x8 array are summarized in Table 5, including the width of the bottom layer microstrip lines. Simulation results for the three arrays are shown in Table 6.

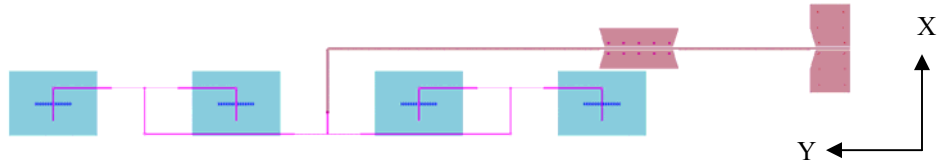


**Figure 17.** Layout of 4x1 array with aperture coupling and T-junctions (RT/Duroid).

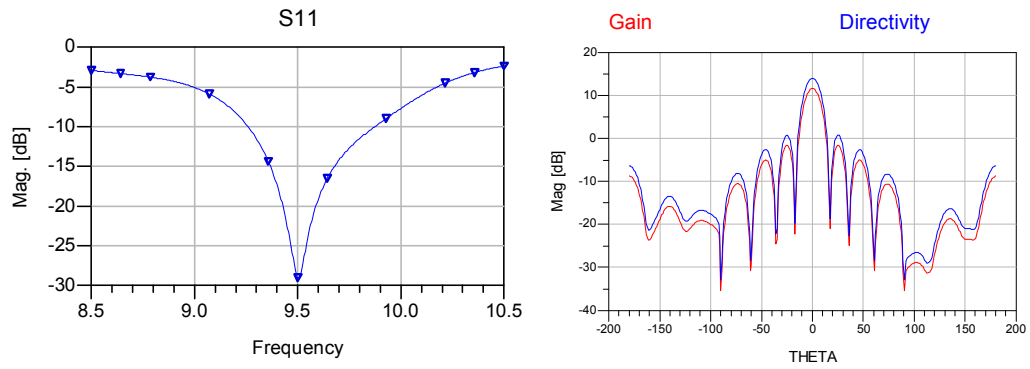


**Figure 18.** Simulated return loss and radiation pattern of 4x1 array with aperture coupling and T-junctions (RT/Duroid).

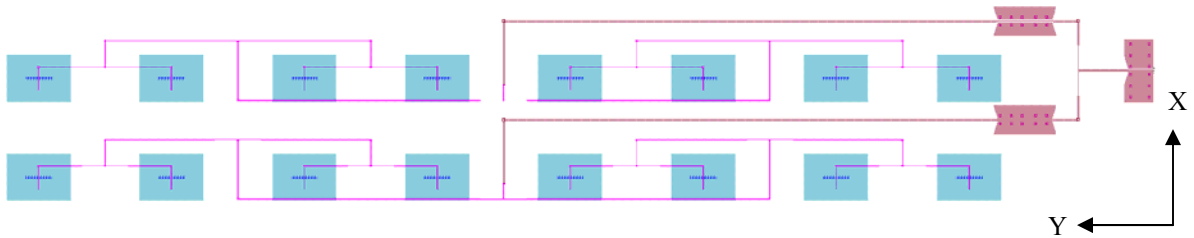


**Figure 19.** Layout of 8x2 array with aperture coupling and T-junctions (RT/Duroid).

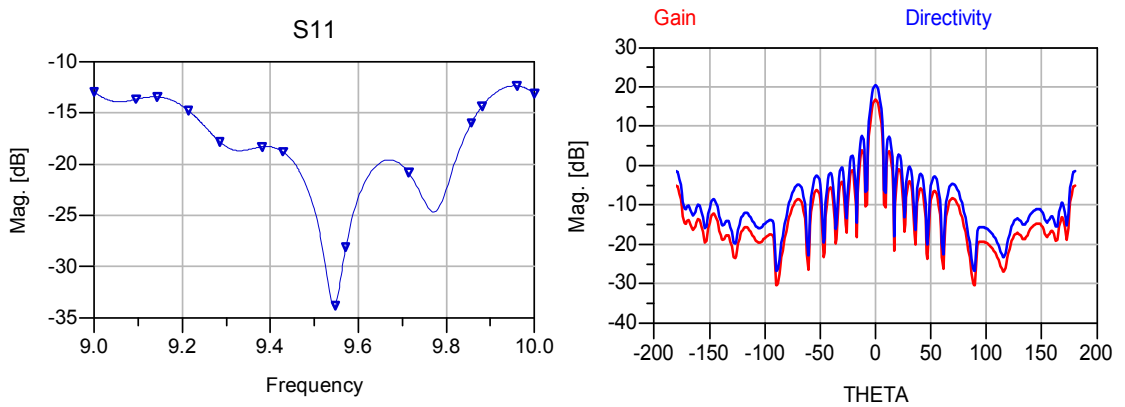


**Figure 20.** Simulated return loss and radiation pattern of 8x2 array with aperture coupling and T-junctions (RT/Duroid).



**Figure 21.** Layout of 8x8 array with aperture coupling and T-junctions (RT/Duroid).

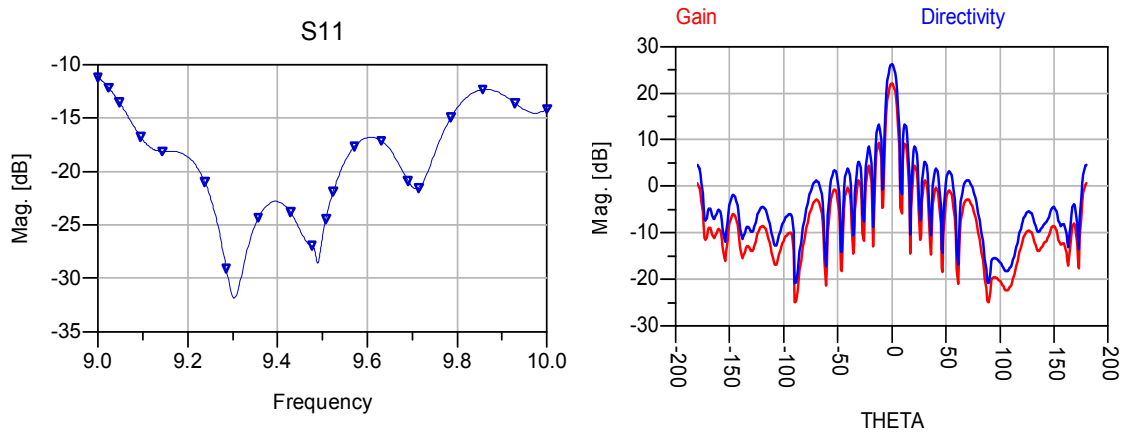


**Figure 22.** Simulated return loss and radiation pattern of 8x8 array with aperture coupling and T-junctions (RT/Duroid).

**Table 5:** Dimensions for 8x8 Array with T-Junctions using RT/Duroid® 5880LZ

Parameter	Value (mm)
50-Ω line width (embedded)	.236
70-Ω line width (embedded)	.125
50-Ω line width (bottom)	.446
70-Ω line width (bottom)	.255
Patch width	12.9
Patch length	9.82
Slot width	.444
Slot length	5.44
Open circuit stub length	2.27

**Table 6:** Simulation Results for Arrays with Aperture Coupling and T-Junctions using RT/Duroid® 5880LZ

	4x1 Array	8x2 Array	8x8 Array
10dB Bandwidth (GHz)	.616	.9	3
Power Gain (dBi)	11	16.68	22.09

### 3.2.2 Via-Fed Antenna Arrays

A single element antenna was designed and simulated, and then used to form arrays. The single patch antenna design starts by assuming a width of  $\lambda/2$

$$W = \frac{c}{2f\sqrt{\epsilon_r}} \quad (27)$$

The length is calculated with equation (13), and this value is used iteratively as the width  $W$  (assuming a square patch) in the equations to recalculate the effective dielectric constant (equation (8)), and then obtain a new resonant length value. The input conductance of the patch fed on the edge is given by twice the conductance of one of the edge slots (equation (9)), so the input resistance at the edge is

$$R_e = \frac{1}{2G} \quad (28)$$

The resistance along the length of the patch is given by

$$R_i = R_e \sin^2 \frac{\pi x}{L} \quad 0 \leq x \leq \frac{L}{2} \quad (29)$$

where  $R_i$  is the input resistance, and  $x$  is the distance from the patch center. The input resistance is then zero in the center and  $R_e$  on the edge of the patch. [5] The feed point is determined by the desired input impedance ( $R_i = 50\Omega$ ) as follows

$$x = \frac{L}{\pi} \sin^{-1} \sqrt{\frac{R_i}{R_e}}. \quad (30)$$

The single element antenna and antenna arrays were simulated with the calculated initial values using Momentum and were then optimized by adjusting the patch dimensions, feed line width, and feed point  $x$ . The material used for the patch substrate is RT/Duroid® 5880LZ. Figure 23 shows the stack-up used for the via-fed antennas including the feeding via, and a shorting pin on the center of each patch. The via goes from the embedded feed network to the patch, and passes through an opening on the ground plane. This opening is roughly twice the diameter of the via, and its necessary to avoid shorting the signal. Figure 24 shows the layout of an 8x8 array, and figure 25 shows the simulated return loss and H-plane radiation pattern. The dimensions for this array are summarized in Table 7; the diameter of the vias is dependent on the fabrication capabilities (fabrication is discussed in the next chapter). The simulation results are on Table 8.

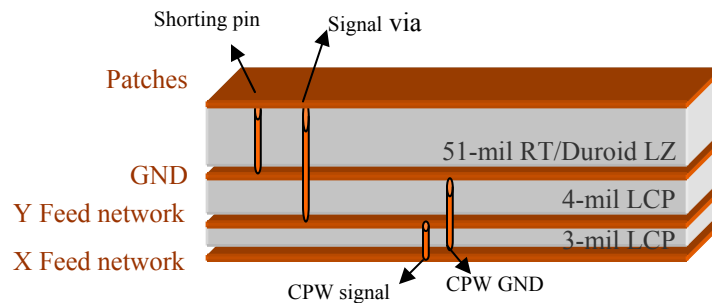


**Figure 23.** Substrate stack-up for via-fed arrays.

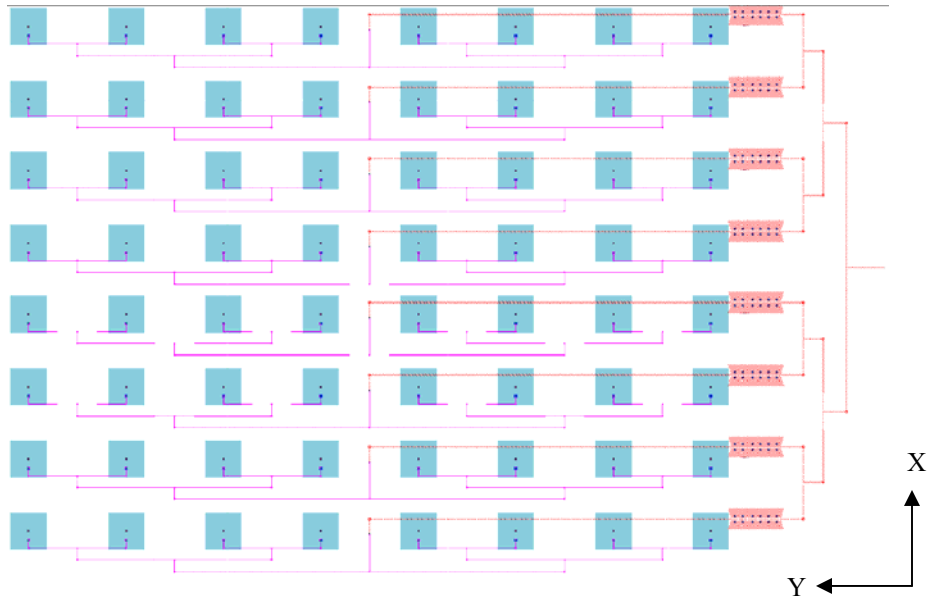


**Figure 24.** Layout of 8x8 array with via feed.

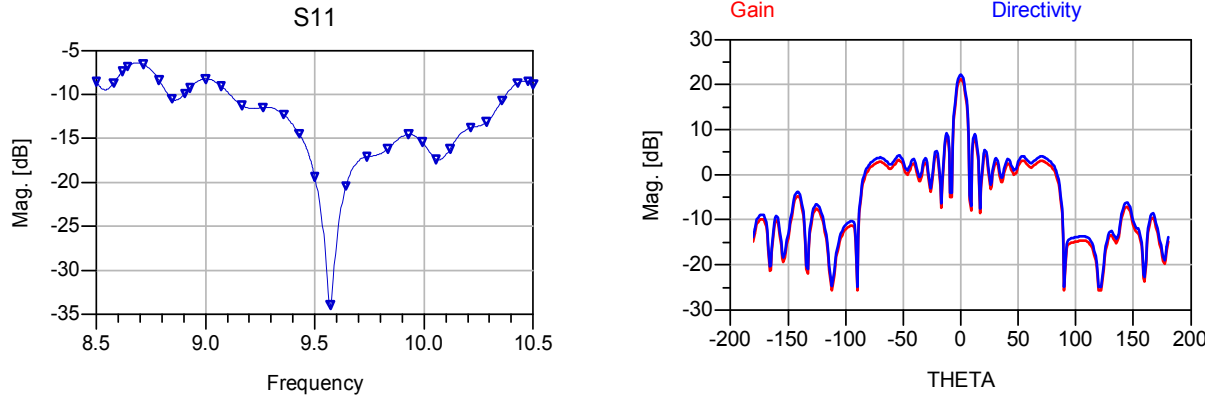


**Figure 25.** Simulation return loss and radiation pattern of 8x8 array with via feed.

**Table 7:** Dimensions for 8x8 Array with Via Feed using RT/Duroid® 5880LZ

<b>Parameter</b>	<b>Value (mm)</b>
50-Ω line width (embedded)	.241
70-Ω line width (embedded)	.128
50-Ω line width (bottom)	.446
70-Ω line width (bottom)	.246
Patch width	10.02
Patch length	10.27
Feed point x (from center)	2.53
Feeding Via and pin diameter	.3

**Table 8:** Simulation Results for 8x8 Array with Via Feed

	<b>8x8 Array</b>
10dB Bandwidth (GHz)	1.27
Power Gain (dBi)	21.2

### **3.3 Antenna Arrays with Corporate Feed Networks using Wilkinson Dividers**

Linear and planar antenna arrays of different sizes were designed with microstrip line feed networks employing Wilkinson power dividers. Figure 26 shows the substrate stack-up used. It is the same as the one used for the arrays using T-junctions, but it has a thin film resistive foil bonded to the 4-mil ULTRALAM 3850 layer, which is used to form the resistors needed to connect the output ports of the Wilkinson dividers. Only the y-direction embedded feed network uses Wilkinson dividers; the feed network on the bottom layer uses T-junctions like in the previous section. The spacing between the microstrip lines in the feed networks is 3 times the line-width to avoid cross coupling. The x and y direction spacing between lines in different layers are also carefully chosen to avoid possible cross coupling and thus optimize the circuit performance. The antenna elements substrate is 51 mils for the X-band arrays designs, and it is 10 mils for the

designs in Ka-band. All the array designs done using Wilkinson dividers use aperture coupling to feed the antenna elements; the slots on the ground plane centered underneath each antenna element can be seen in Figure 26. The aperture coupled antenna design is described in section 3.2.1.

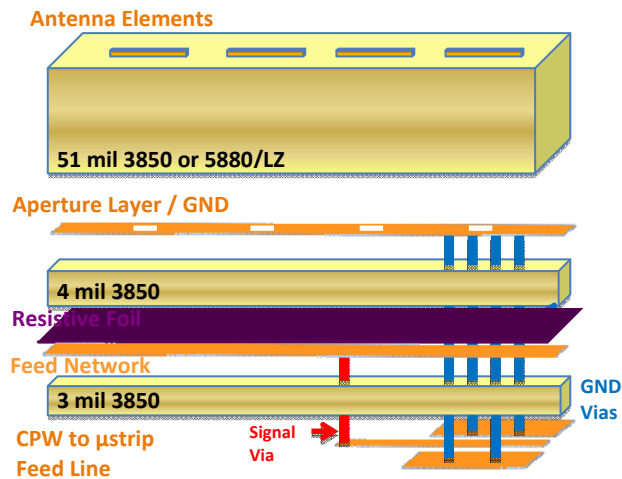


**Figure 26.** Substrate stack-up for aperture coupled antenna arrays.

Having the resistors embedded as opposed to surface-mounted is advantageous because parasitic effects are reduced, and because the size of the resistor can be scaled as needed by the circuit layout. Each Wilkinson divider used in the feed network has equal power splits. Figure 27 shows the layout of one of these dividers, where a bend radius as large as possible is used for the quarter wave lines. In planar form, a common problem found designing the Wilkinson divider is separating the quarter-wave transformers to avoid mutual coupling, while keeping them close enough to place a resistor between them. The 4-mil substrate used to realize the Wilkinson dividers is thin enough to allow for smaller line-widths, making this layout feasible, yet not too thin to introduce significant losses. [6]

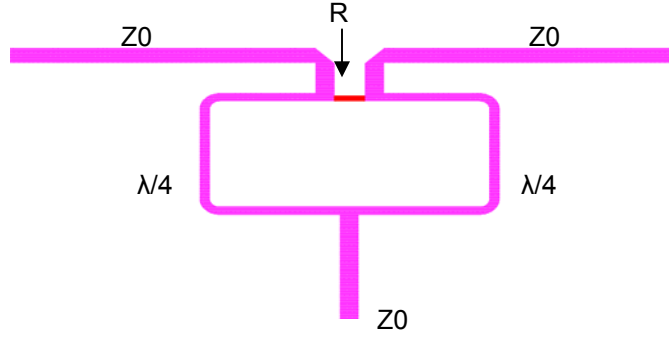


**Figure 27.** Layout of Wilkinson divider used in embedded RF feed network.

The characteristic impedance  $Z_0$  is  $50 \Omega$ , and the impedance of the quarter wave lines is  $\sqrt{2} * Z_0$ , which is  $70.7 \Omega$ . Using the desired impedance, the line widths are found with the microstrip line formulas in equation (25). The electrical length of the quarter-wave lines is dependent on the effective wavelength, and therefore the resonant frequency, as follows

$$\beta l = \frac{2\pi}{\lambda} \frac{\lambda}{4} = \frac{\pi}{2} \text{ rad}; \quad (31)$$

the physical length is then given by

$$l = \frac{\frac{\pi}{2}}{\sqrt{\epsilon_{\text{reff}}} k_0}. \quad (32)$$

The value of the resistor must be  $R = 100 \Omega$ . This value, together with the resistivity of the thin film used ( $\rho = 25 \Omega/\square$ ), determines the dimensions of the resistor as follows

$$\frac{A}{l} = \frac{\rho}{R}; \quad (33)$$

since the thickness of the resistive foil is negligible, the value of the cross-sectional area  $A$  determines the width of the resistor. Due to fabrication tolerances, the larger the resistors are made, the more accurate the resistance values are. The length and width of the resistor were initially chosen to be .4 mm and .1 mm respectively, but were later slightly modified due to fabrication constraints. The fabrication of embedded resistors is described in the next chapter.

### 3.3.1 X-Band Antenna Arrays

The antenna arrays with Wilkinson dividers designed for X-band have the same specifications as the arrays with T-junctions described in the previous section, with a center frequency of 9.5 GHz, and bandwidth of 500 MHz, y-direction spacing of 27 mm and x-direction spacing of 20 mm. The radiating patches substrate layer is ULTRALAM 3850 for the first design shown and RT/Duroid® 5880LZ for the rest.

#### 3.3.1.1 Antenna Arrays using ULTRALAM 3850

The design layout and Momentum simulation results for an 8x1 array using ULTRALAM 3850 for all the substrate layers are shown in Figures 28 and 29 respectively. The CPW lines on the bottom metal layer are not included. The dimensions for the antennas and feed network are listed in Table 9, and the simulation results are in table 10.

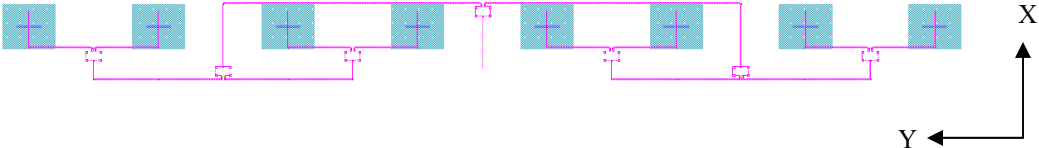


**Figure 28.** Layout of X-band 8x1 array with Wilkinson dividers (ULTRALAM).

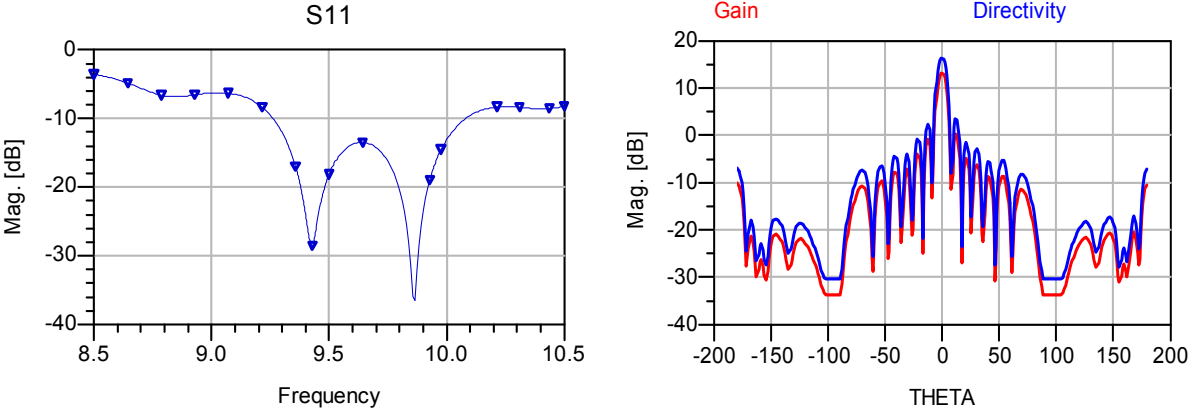


**Figure 29.** Simulated return loss and radiation pattern of X-band 8x1 array with Wilkinson dividers. (ULTRALAM).

**Table 9:** Dimensions for X-Band 8x1 Array with Wilkinson Dividers using ULTRALAM 3850

Parameter	Value (mm)
50-Ω line width	.254
70-Ω line width	.138
Patch width	11.11
Patch length	8.77
Slot width	.523
Slot length	5.23
Open circuit stub length	2.73

**Table 10:** Simulation Results for X-Band 8x1 Array with Wilkinson Dividers using ULTRALAM 3850

	8x1 Array
10dB Bandwidth (MHz)	821
Power Gain (dBi)	13.22

### 3.3.1.2 Antenna Arrays using RT/Duroid® 5880LZ

Antenna arrays of different sizes were also designed using RT/Duroid® for the radiating patches substrate. Figures 30 through 33 show the layout and Momentum simulation results for a 4x1 and an 8x8 array. The dimensions for the 8x8 array are listed in Table 11. The simulation results for the two arrays are summarized in Table 12.

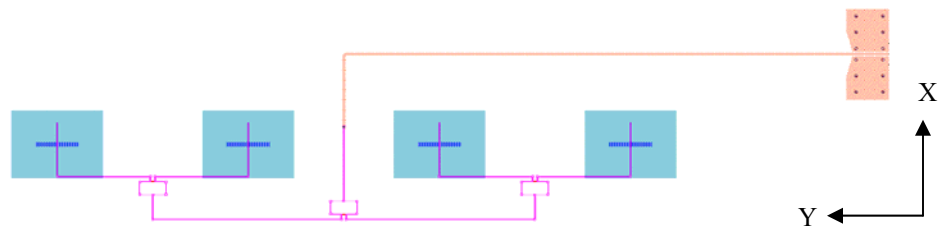


**Figure 30.** Layout of X-band 4x1 array with Wilkinson dividers (RT/Duroid).

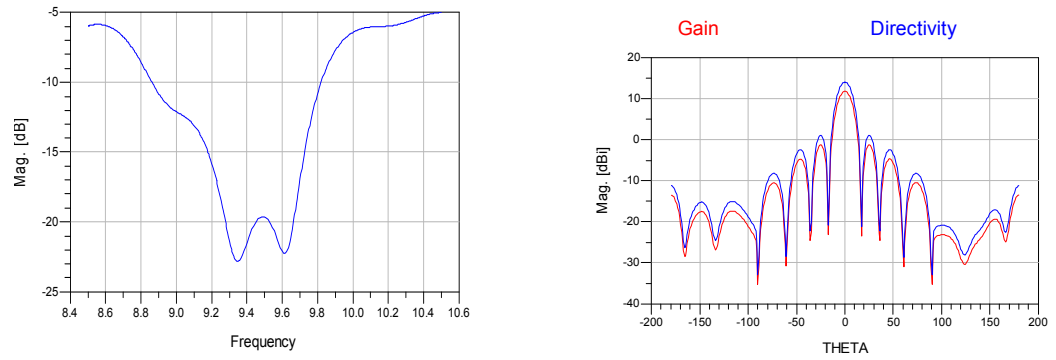


**Figure 31.** Simulated return loss and radiation pattern of X-band 4x1 array with Wilkinson dividers (RT/Duroid).

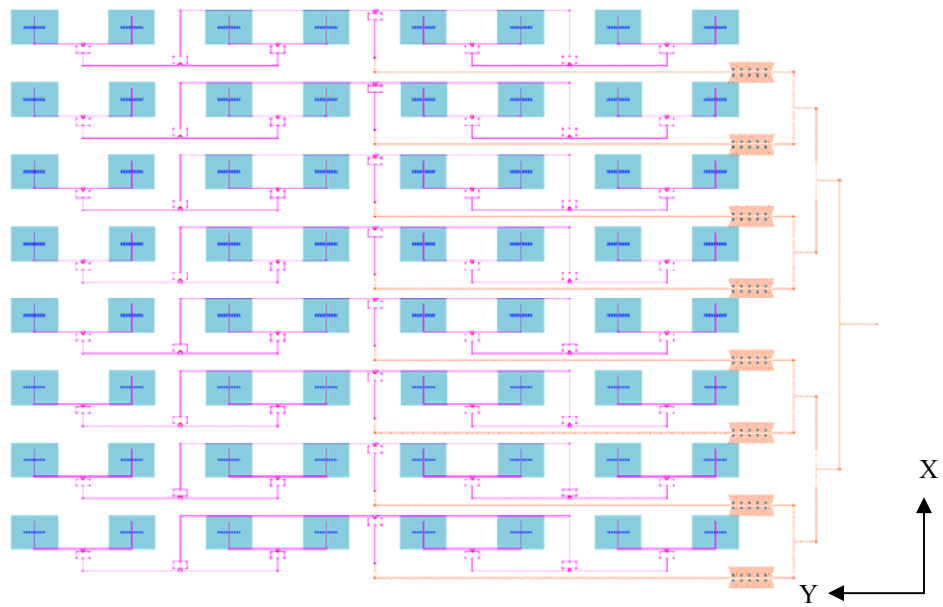


**Figure 32.** Layout of X-band 8x8 array with Wilkinson dividers (RT/Duroid).

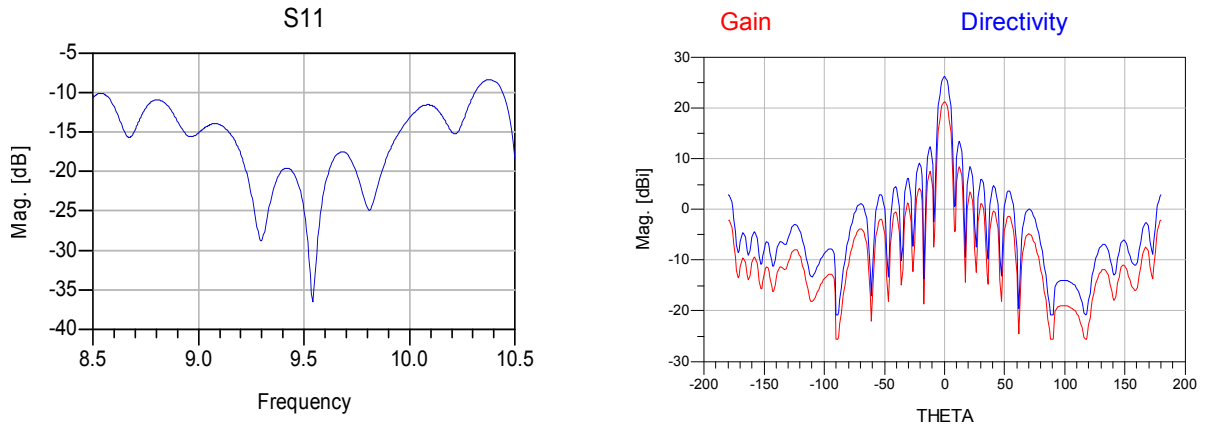


**Figure 33.** Simulated return loss and radiation pattern of X-band 8x8 array with Wilkinson dividers. (RT/Duroid).

**Table 11:** Dimensions for X-Band 8x8 Array with Wilkinson Dividers using RT/Duroid® 5880LZ

Parameter	Value (mm)
50-Ω line width (embedded)	.253
70-Ω line width (embedded)	.139
50-Ω line width (bottom)	.446
70-Ω line width (bottom)	.254
Patch width	12.98
Patch length	9.61
Slot width	.614
Slot length	6.27
Open circuit stub length	2.86

**Table 12:** Simulation Results for X-Band Arrays with Wilkinson Dividers using RT/Duroid® 5880LZ

	4x1 Array	8x8 Array
10dB Bandwidth (GHz)	.955	1.85
Power Gain (dBi)	8.96	21.29



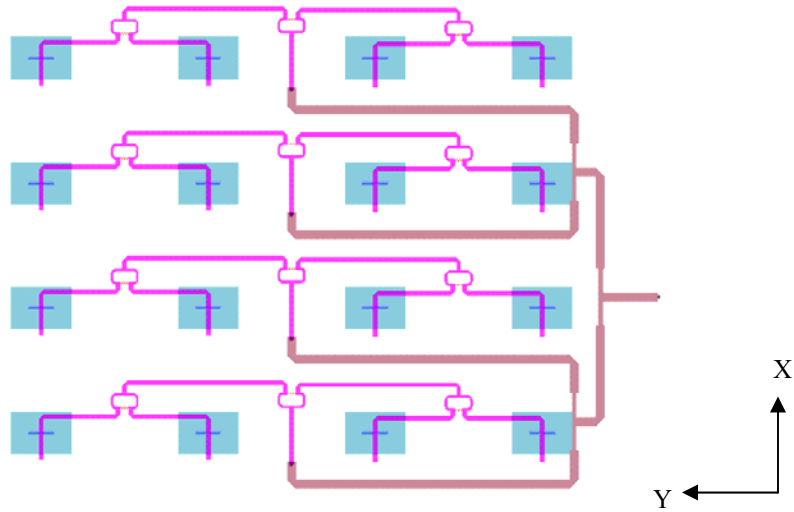


**Figure 35.** Layout of 4x4 Ka-band array with Wilkinson dividers (RT/Duroid).

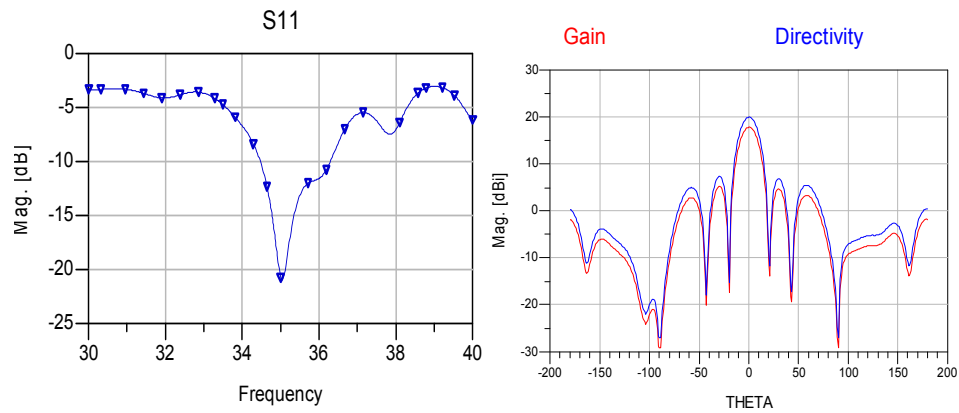


**Figure 36.** Simulated return loss and radiation pattern of Ka-band 4x4 array with Wilkinson dividers. (RT/Duroid).

**Table 13:** Dimensions for Ka-Band 4x4 Array with Wilkinson Dividers using RT/Duroid® 5880LZ

Parameter	Value (mm)
50-Ω line width (embedded)	.245
70-Ω line width (embedded)	.131
50-Ω line width (bottom)	.442
70-Ω line width (bottom)	.238
Patch width	3.07
Patch length	2.15
Slot width	.13
Slot length	1.3
Open circuit stub length	1.46

**Table 14:** Simulation Results for Ka-Band Arrays with Wilkinson Dividers using RT/Duroid® 5880LZ

	<b>4x4 Array</b>
10dB Bandwidth (GHz)	1.82
Power Gain (dBi)	17.84

### **3.4 Antenna Phased Array Beam Steering**

The planar arrays described in the previous section are intended to be used as phased arrays. The goal is to steer the main beam in the x-direction by a maximum angle of 20° off broadside. Each 8x1 row on the planar array is taken as one element, and since the spacing between the elements is fixed, the beam is steered by changing the phase difference between elements as mentioned in section 2.3.1. The phase difference is changed with the use of surface-mount phase shifters integrated on the CPW that is printed on the bottom layer of the antenna substrate. Since one 8x1 row is considered one element, only one phase shifter is needed per row. Therefore, in an 8x8 array, there are 8 phase shifters, and each 8x1 row has a different phase.

Table 15 shows the phases achieved by the 3-bit phase shifter used. The values in black are ideal, and the values in red are the actual values measured. As explained in section 2.3.1, having a progressive phase shift  $\alpha$  between elements of the array, causes the main beam to be directed at a certain angle  $\theta$  from the  $\alpha = 0$  position, which in the case of microstrip antennas, is the broadside position. Appendix B shows the predicted beam steering angles for an X-band 8x8 array when the distance between elements is 20 mm, and the progressive phase difference  $\alpha$  takes some of the values listed in Table 15. The plots show the magnitude of the total array electric field at different  $\alpha$  values. The plots were generated with MATLAB using the equations of section 2.3.1, and the simulated E-field magnitude of an 8x1 array with T-junctions (on RT/Duroid® substrate) as the electric field of a single element. The main beam steers about 45° when  $\alpha$  varies from 0 to 169°.

**Table 15:** Values of Phase Shift  $\alpha$  Obtained from Phase Shifter

State Number	Bit State	Phase Shift
1	[0,0,0]	0
2	[1,0,0]	45 (42)
3	[0,1,0]	90 (89)
4	[1,1,0]	135 (131)
5	[0,0,1]	180 (169)
6	[1,0,1]	225 (211)
7	[0,1,1]	270 (259)
8	[1,1,1]	315 (303)

## CHAPTER 4

### FABRICATION AND MEASUREMENT RESULTS

Some of the microstrip antenna arrays described in the previous chapter, were fabricated, and their s-parameters and far field radiation were measured and calculated. Results for both baseline antenna arrays and antenna arrays with integrated surface-mount active devices such as phase shifters and amplifiers, are presented here .

#### 4.1 Fabrication

The arrays were fabricated by external vendors using low cost printed circuit board techniques. A photolithographic etch process is used to form the structures on each layer. When all the layers are complete, the stack is bonded together using thermal compression at a temperature at which only the ULTRALAM bonding film (low-melt LCP) melts. When this temperature is reached, pressure is applied to break the molecular bonds of the low-melt LCP, and create new bonds with the substrate material (high-melt LCP or Duroid). [14] The larger vias are created with a mechanical drill, while the smaller ones are created with a laser. The vias are filled with a thin layer of copper by using either sputtering or electroless plating; then they are completely filled using electroplating. Since the arrays use a multilayer substrate and a flexible material (LCP), alignment is a very crucial step in the fabrication. Two types of alignment marks are used on each layer: pinhole alignment marks on the corners and cross marks along the edges. [3] Redundancy in the alignment marks is necessary because there is no guarantee that the pinholes will be exactly the same size.

The fabrication capabilities and tolerances put a limit on the feature sizes. The minimum feature size depends on the thickness of the copper. For both ULTRALAM and RT/Duroid®, the copper is ½ oz. The minimum feature size for ½ oz copper has

been determined to be 75  $\mu\text{m}$  for traces and 50  $\mu\text{m}$  for slots. While smaller features are possible, these are the smallest features that can be reproduced accurately. [15] It is convenient to oversize the line-widths on the mask to account for over-etching during the fabrication process. The fabrication process also limits the size of the vias. The design rule for industry standards is to have the via hole diameter be twice as large as its vertical length. This rule was followed in the design of the antenna arrays to ensure good connections. In addition, the vias need a large enough pad around them (usually twice the via diameter) to ensure good contact between the layers and compensate for misalignment. This pad in the feed network introduces parasitic capacitance, and can change the impedance of the feed line. Therefore, a tradeoff is encountered between good impedance matching, and good connection between layers. Simulations were performed with different via-pad sizes, to find a convenient diameter. The feed networks were optimized to account for the effects of the via pads. [14]

The embedded resistors needed for the Wilkinson dividers are realized with a commercially available resistive foil laminated to the 4-mil LCP substrate. This provides a low cost manufacturing solution. Resistors are formed using an etching process after lamination. Since the resistance value is highly dependent on the physical dimensions, uniformity needs to be tightly controlled. Using the embedded foil eliminates the need to control the thickness of the lines, leaving only the length and width to be defined by the etching process. The process for forming embedded resistors is depicted in Figure 37. In Figure 37a, the sample is shown with the resistor foil bonded to the LCP. After defining a pattern with a photoresist mask, the copper and thin film resistor underneath the copper are etched in a single bath as seen in Figure 37b. A second photoresist mask followed by a selective copper etch exposes the thin film resistors and completes the formation of the layer as shown in Figure 37c. The resistor layer thus defined will be embedded in the multilayer antenna design. [16]

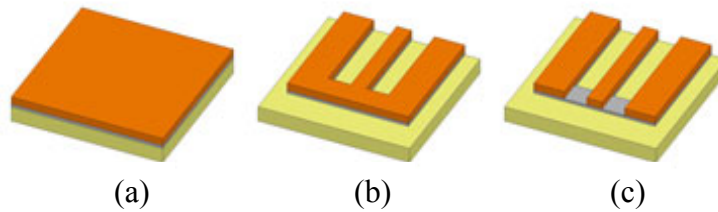


**Figure 37.** Process for fabricating embedded resistor for Wilkinson power divider; (a) laminated resistor on LCP, (b) patterned Cu and resistor, (c) resistor with copper terminal pads.

The resistors designed for the Wilkinson dividers were  $100\mu\text{m} \times 400\mu\text{m}$ ; however, for the fabrication the dimensions were changed to  $76.4\ \mu\text{m} \times 305.6\ \mu\text{m}$ . For a film resistivity of  $25\ \Omega/\square$ , these dimensions should still provide a resistance of  $100\ \Omega$ . The fabricated resistors for the Wilkinson dividers are shown in figure 38.

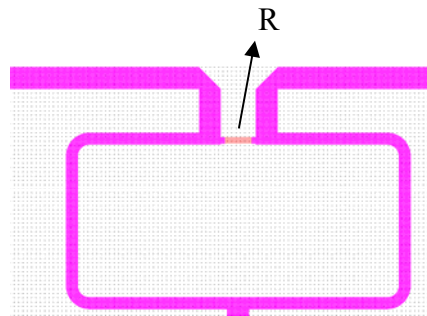


**Figure 38.** Layout of Wilkinson divider with embedded resistor as fabricated.

The mask layouts and fabricated  $8 \times 8$  and  $4 \times 1$  arrays with T-junctions are shown in Figure 39. Only the top (antenna elements) and bottom (x-direction feed network) layers are shown since the other two layers (ground and y-direction feed network) are embedded.

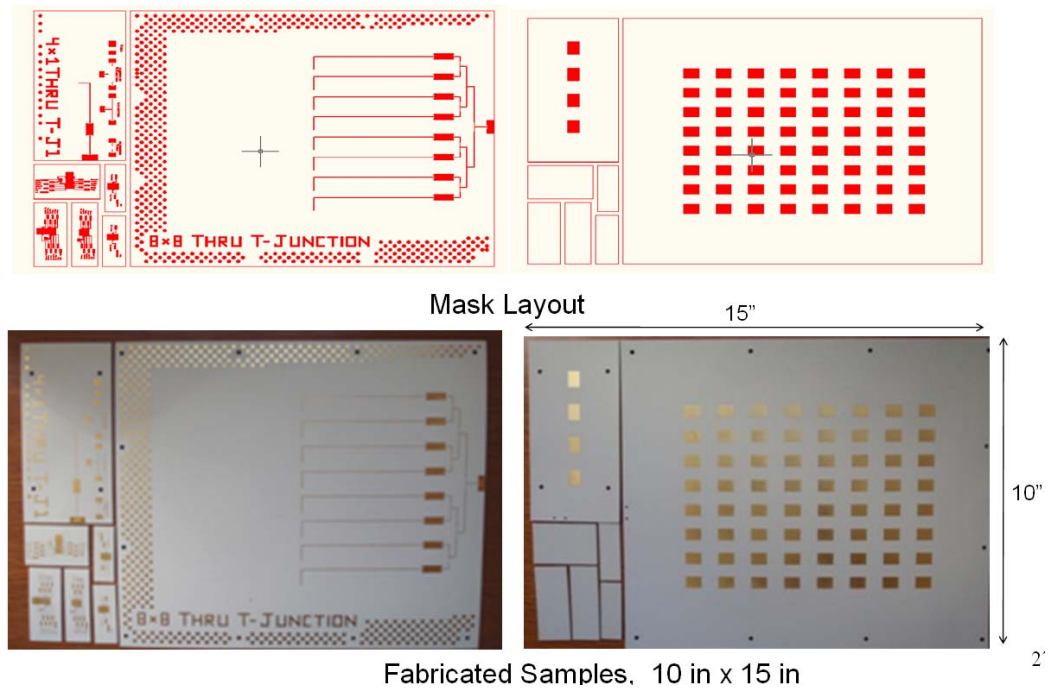


**Figure 39.** Mask layout and fabricated antenna arrays.

## 4.2 Measurement results

The measured S-parameters and radiation patterns of the fabricated antenna arrays are presented here, and comparisons are made with simulation data. Data including integrated amplifiers and phase shifters is also included. The s-parameter measurements were performed using the probe station, RF probes and cables, and PNA at the Georgia Tech MircTech lab. Radiation measurements were performed using the anechoic chamber at GTRI. Figure 40 shows a picture of the anechoic chamber test set-up for an 8x8 receive array, in which SiGe electronics (LNAs and phase shifters) were wire-bonded to the CPW line on the bottom layer of the antenna substrate. Figure 41 shows the near field range measurement performed. A waveguide probe scans the elevation while the antenna rotates to capture the full antenna pattern. The antenna array can be electronically scanned in the azimuth direction.

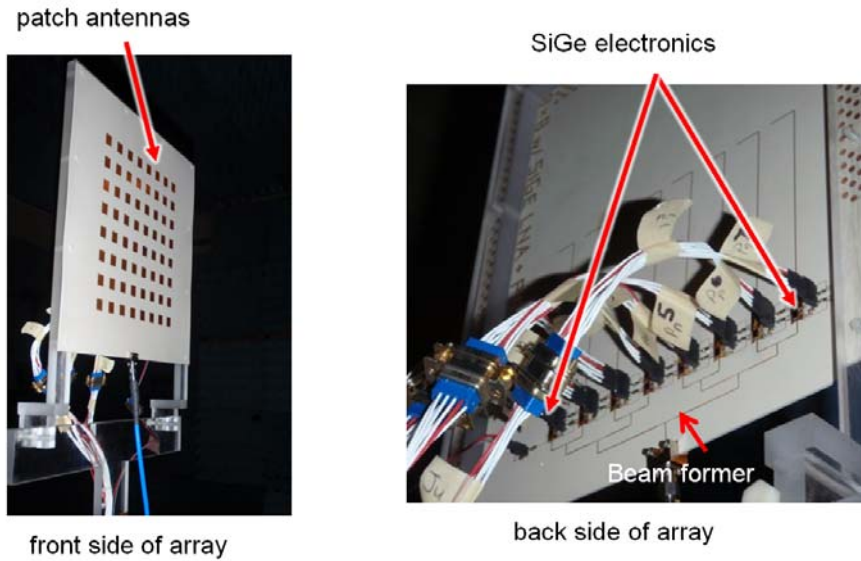


**Figure 40.** Photos of front and back side of receive 8x8 array during radiation measurement.



**Figure 41.** NFR scan of 8x8 antenna array.

#### 4.2.1 Measured Results for Arrays using ULTRALAM 3850

The measured return loss for the 4x1 and 8x1 arrays with aperture coupling and feed networks using T-junctions described in section 3.2.1.1 are shown in Figure 42. The 4x1 array results include the baseline as well as the array with integrated LNA [17]. The

8x1 array results include the array with integrated LNA and the array with LNA and phase shifter [18]. The measured radiation patterns for the 4x1 antenna array are shown in Figure 43 and compared to Ansoft HFSS simulations. The measured radiation patterns for the 8x1 array with integrated LNA are shown in Figure 44 and compared to HFSS simulations. The difference in gain with the simulations presented in section 3.2.1.1 is due to the extra gain provided by the LNA.

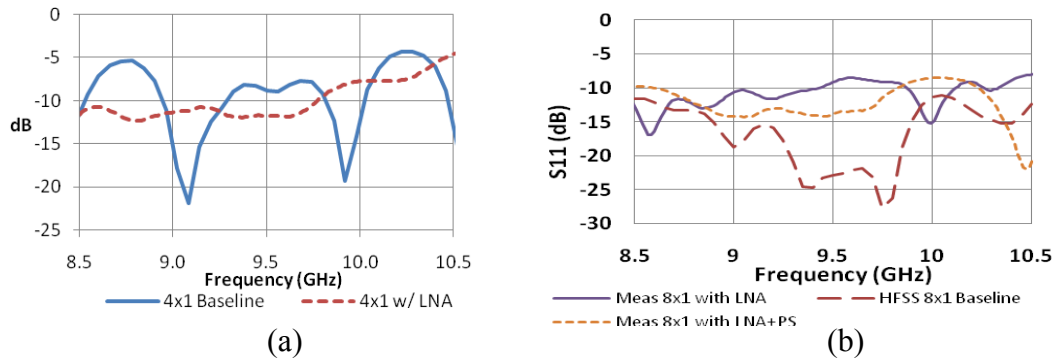


**Figure 42.** Measured return loss of (a) 4x1 and (b) 8x1 antenna arrays (ULTRALAM 3850).

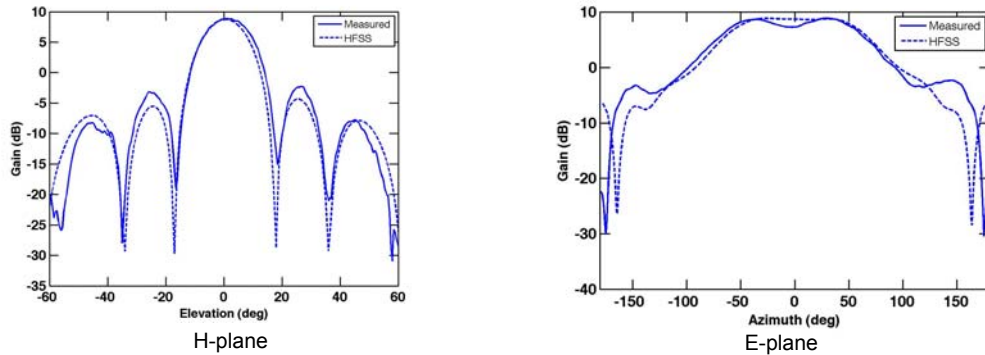


**Figure 43.** Measured vs. simulated radiation patterns for 4x1 array (ULTRALAM 3850).

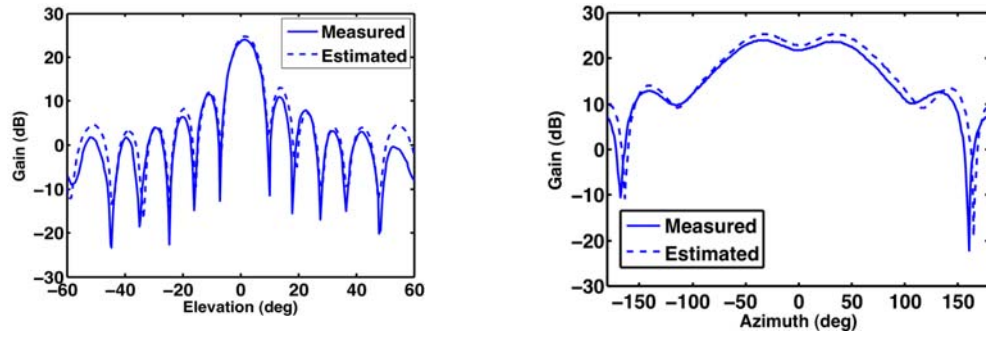


**Figure 44.** Measured vs. simulated radiation patterns for 8x1 array with integrated LNA (ULTRALAM 3850).

#### 4.2.2 Measured Results for Arrays using RT/Duroid® 5880LZ

##### 4.2.2.1 Antenna Arrays with Feed Networks using T-Junctions

The measured return loss of the 4x1 aperture-coupled array with feed network using T-junctions described in section 3.2.1.2, is displayed in Figure 45 and compared to the Momentum simulated data, where the blue trace is the simulated S11 and the red trace is the measured S11. Figure 46 shows the measured vs. HFSS simulated radiating patterns for the 4x1 array.

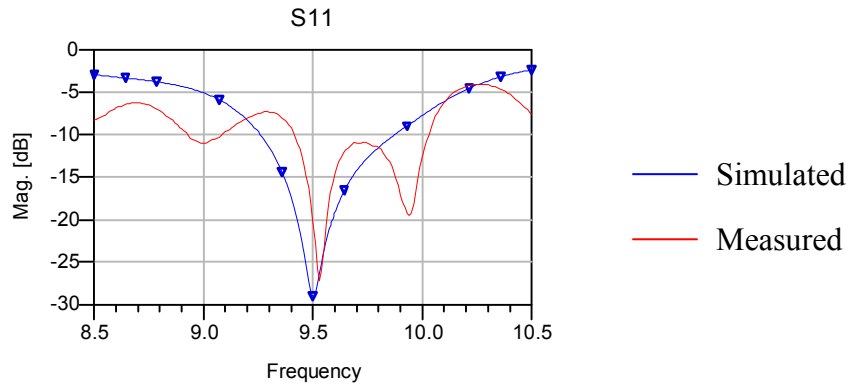


**Figure 45.** Measured vs. simulated return loss of 4x1 array with feed network using T-junctions (RT/Duroid® 5880LZ).

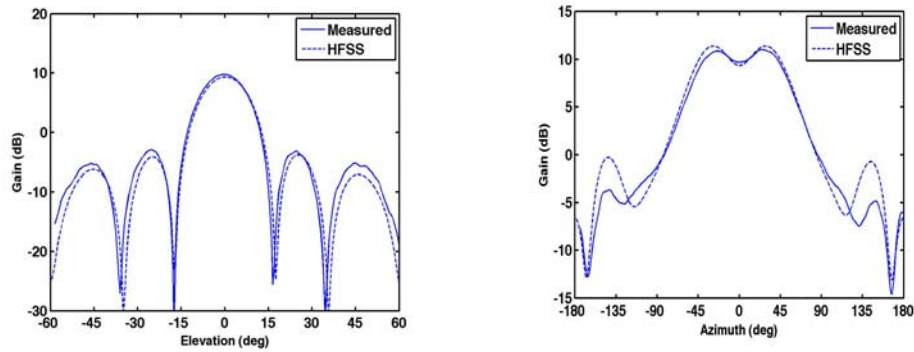


**Figure 46.** Measured vs. simulated radiation patterns for 4x1 array with T-junctions (RT/Duroid® 5880LZ).

Figure 47 shows the measured return loss of the aperture coupled 8x1 array with feed network using T-junctions. Measurements of a baseline array as well as an array with integrated SiGe LNA and phase shifter are compared to the HFSS simulation [19]. Figure 48 shows the measured versus simulated radiation patterns. Figure 49 shows the measured versus simulated return loss for the aperture-coupled 8x8 array with feed network using T-junctions. Figure 50 shows the measured versus simulated radiation patterns for the 8x8 array.

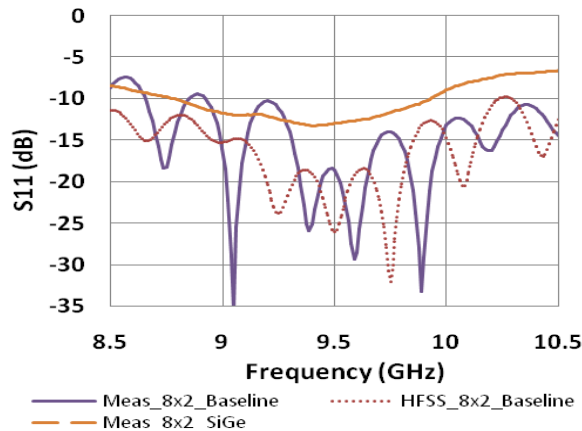


**Figure 47.** Measured vs. simulated return loss of 8x2 array with feed network using T-junctions (RT/Duroid® 5880LZ).

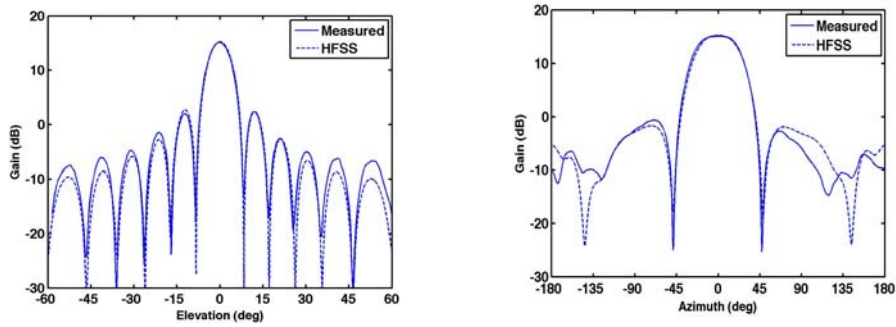


**Figure 48.** Measured vs. simulated radiation patterns for 8x2 array with T-junctions (RT/Duroid® 5880LZ).

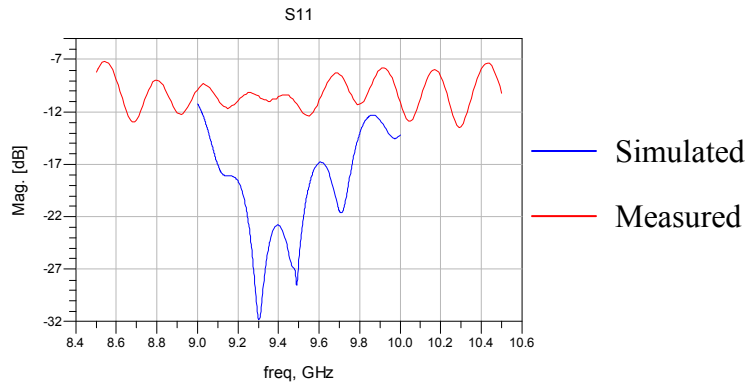


**Figure 49.** Measured vs. simulated return loss of 8x8 array with feed network using T-junctions (RT/Duroid® 5880LZ).

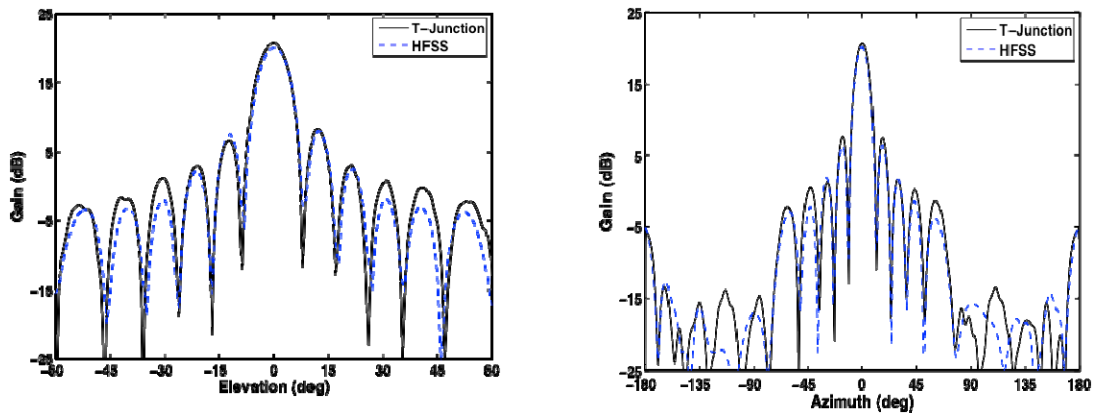


**Figure 50.** Measured vs. simulated radiation patterns for 8x8 array with T-junctions (RT/Duroid® 5880LZ).

#### 4.2.2.2 Antenna Arrays with Feed Networks using Wilkinson Dividers

The actual values of the fabricated resistors for the Wilkinson dividers were approximately  $130\ \Omega$  for the 4x1 array and  $136\ \Omega$  for the 8x8 array described in section 3.3.1.2. These values are the average of the different resistances obtained from test resistors fabricated on the same board as the arrays. Simulations were performed again to account for the difference in resistance values, in order to compare with the measured data (simulation data shown in section 3.3.1.2 reflect this change in resistance). The measured versus simulated return loss of the 4x1 array are shown in Figure 51, and the measured radiation patterns are shown in Figure 52. The measured versus simulated return loss for the 8x8 array are shown in Figure 53. The measured radiation patterns are shown in Figure 54, and are compared to the simulation data as well as the measured data for the 8x8 array with feed networks using T-junctions.

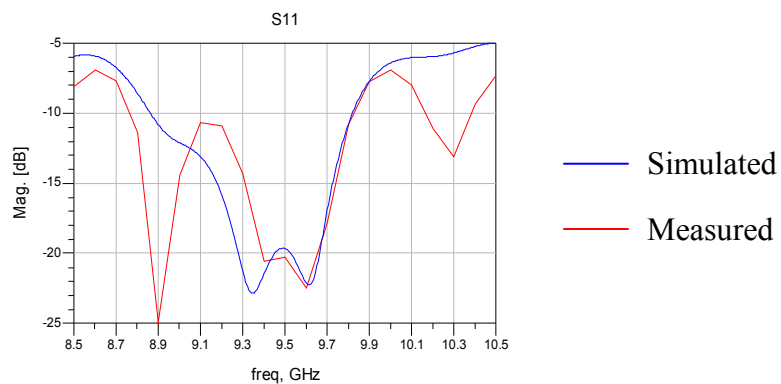


**Figure 51.** Measured vs. simulated return loss for 4x1 array with Wilkinson dividers (RT/Duroid® 5880LZ).

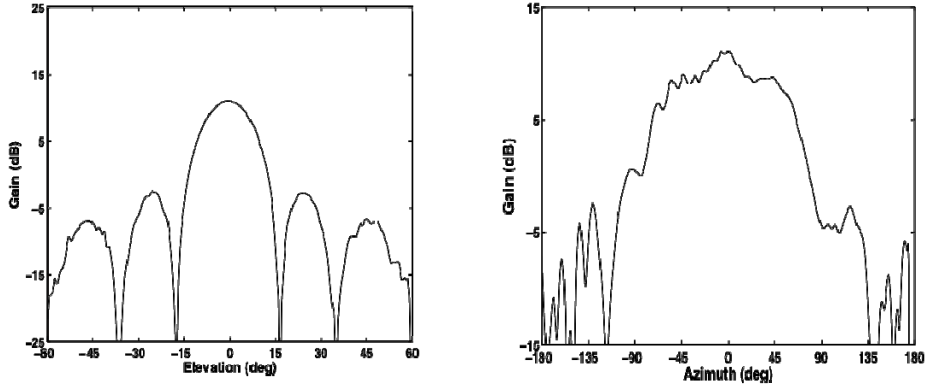


**Figure 52.** Measured vs. simulated radiation patterns for 4x1 array with Wilkinson dividers (RT/Duroid® 5880LZ).

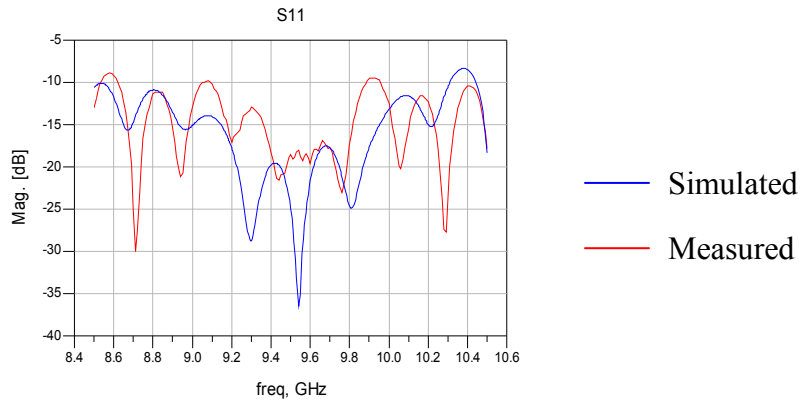


**Figure 53.** Measured vs. simulated return loss for 8x8 array with Wilkinson dividers (RT/Duroid® 5880LZ).

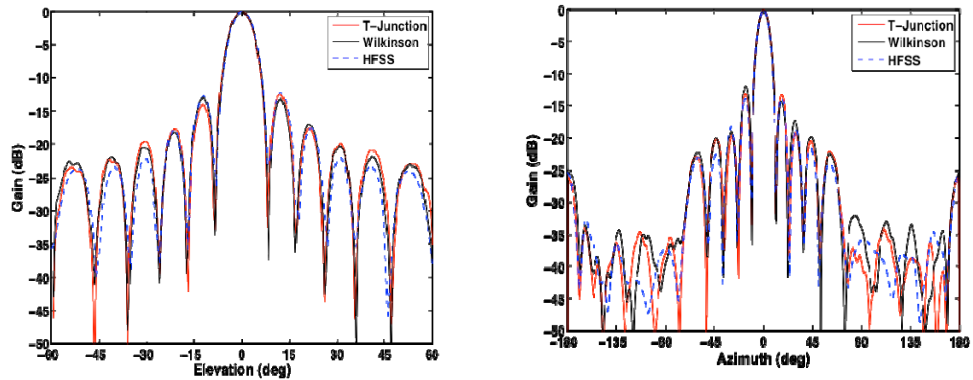


**Figure 54.** Measured vs. simulated normalized radiation patterns for 8x8 array with Wilkinson dividers (RT/Duroid® 5880LZ).

### 4.2.3 Antenna Array Beam Steering

Figure 55 shows the measured versus simulated radiation patterns obtained from the 8x8 array with feed networks using T-junctions, for different phase shifts. Antenna scan angles go from  $\theta = \pm 26^\circ$  with side-lobe levels better than -10 dB from the main beam. Grating lobes started to appear at  $\theta = \pm 37^\circ$ .

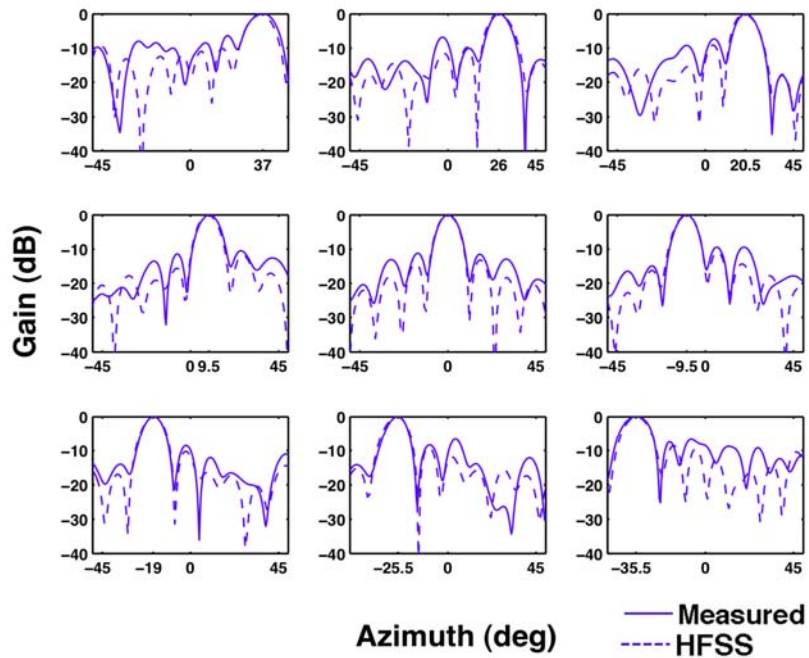


**Figure 55.** Measured radiation patterns for 8x8 array with T-junctions at different phase shift values.

## CHAPTER 5

### ANTENNA ARRAYS APPLICATIONS AND CONCLUSIONS

#### 5.1 Antenna Arrays in Environmental Sensing

The popularity of Active Electronically Scanned Array (AESA) radars grows stronger and stronger, calling for the development of high performance, low cost phased array antennas [20]. The antenna arrays presented in this work can be used as sub-arrays to form a large ESA. One application of ESAs is Measurements in Snow and Cold Land Processes (SCLP), which have gained attention in the recent years due to concerns about global warming and melting of the earth's ice caps. Ice covers more than 25M Km<sup>2</sup> on sea and land; important measurements include snow accumulation, snow-melt, snow-water equivalent (SWE), and water storage in snow. The antennas required for remote sensing applications such as SCLP must have high directivity, low side lobe levels, low loss, and steering capabilities.

Results from the Cold Land Processes Experiment (CLPX) and other studies have demonstrated that characteristics such as SWE exhibit significant spatial variation at scales on the order of 100 m. SWE is the total amount of frozen or liquid water contained in a unit area of snow cover – a function of snowpack depth and density. NASA capabilities are limited to coarse-resolution microwave sensors, such as the Advanced Microwave Sounding Radiometer (AMSR-E). The resolution of these sensors far exceeds the spatial variation of SWE and associated physical processes. This increases the measurement uncertainty, and constrains NASA's capability to assess and understand the variability of critical cold-region characteristics and their effects on local, regional, and global water and energy cycles. To significantly improve the accuracy of remotely sensed snow measurements, resolutions of 100 m or better are necessary. A space-borne microwave

remote sensing approach capable of achieving this resolution is active radar, and research shows great potential for retrieving snowpack properties using this approach. [21]

The planar antenna arrays described in this work can be used as sub-arrays of a SAR (Synthetic Aperture Radar) antenna. SAR is a form of radar in which multiple radar images are processed to yield higher-resolution images than would be possible by conventional means. This can be achieved by mounting the antenna on a moving platform, such as an airplane, to illuminate a relatively stationary target. The many echo waveforms received at the different antenna positions are post-processed to resolve the target. This approach requires the antenna structures to be compact size, lightweight, highly integrated, and tolerant to radiation. [21] The antennas presented in this work meet these requirements, and they also offer a feasible solution since they use a low cost technology.

## **5.2 Conclusions**

Multilayer microstrip antenna arrays intended to be used as phased arrays for environmental sensing radar applications have been presented. A multilayer SOP approach was chosen to achieve a low cost, small size and weight, and high performance system. The materials used for the antenna 3D substrate, Rogers ULTRALAM 3850 (LCP) and Rogers RT/Duroid® 5880LZ, were chosen in order to meet these requirements. The antenna arrays are compatible with active RF electronics that are surface-mounted on the bottom layer CPW line, and enable the operation of the phased array antenna. Antennas in X-band and Ka-band were designed and simulated. The thickness of the antenna elements substrate material was chosen based on the desired antenna 10dB bandwidth (5%), and determined by the operating frequency. The X-band antennas required a 51-mil thick substrate layer while the Ka-band antennas required a 10-mil thick layer. The substrate thickness was a constraint when choosing the antenna elements substrate material, due to limited material availability in certain thicknesses. S-

parameter and radiation pattern measurements of fabricated X-band antennas were presented and compared to ADS/Momentum and HFSS simulations, with very good correlation. Generally, HFSS produced more accurate simulations, which is expected, given that it is a full-wave (3D) EM simulator, while ADS/Momentum is only 2.5D. However, Momentum simulations were accurate enough to predict the general behavior of the antennas, and they were much faster than HFSS simulations.

The multilayer nature of the antenna arrays allowed for independent optimization of the radiating elements and the RF feed networks. This approach also allowed for a much denser layout since cross coupling between lines was not a big concern being that the lines are in different metal layers. In addition, having the ground plane embedded in between the radiating patches and the feed lines minimizes interference of spurious radiation [1]. Two feeding mechanisms that take advantage of the multilayer approach are aperture coupling and via feed. Both methods were studied. The via-fed arrays had a smaller bandwidth and slightly lower gain than the aperture coupled arrays; however their side lobe levels were much lower due to the lower spurious radiation; and the efficiency (gain/directivity) was higher.

Corporate RF feed networks were used to evenly distribute the power to the array elements. Two types of power dividers were studied, reactive T-junctions and Wilkinson power dividers. The T-junctions are simpler to fabricate, and are lossless, but they provide no isolation between the output ports. The Wilkinson dividers involve more complicated fabrication, and they are not completely lossless since reflected power is dissipated in the resistor. However Wilkinson dividers provide isolation between output ports, which prevents mismatches and reflected signals on one output port from propagating to other parts in the system. The resistor used for the Wilkinson dividers was realized with an embedded thin film resistive foil. Having an embedded resistor introduces far fewer parasitic effects than a resistor contained in a separate package. [22]

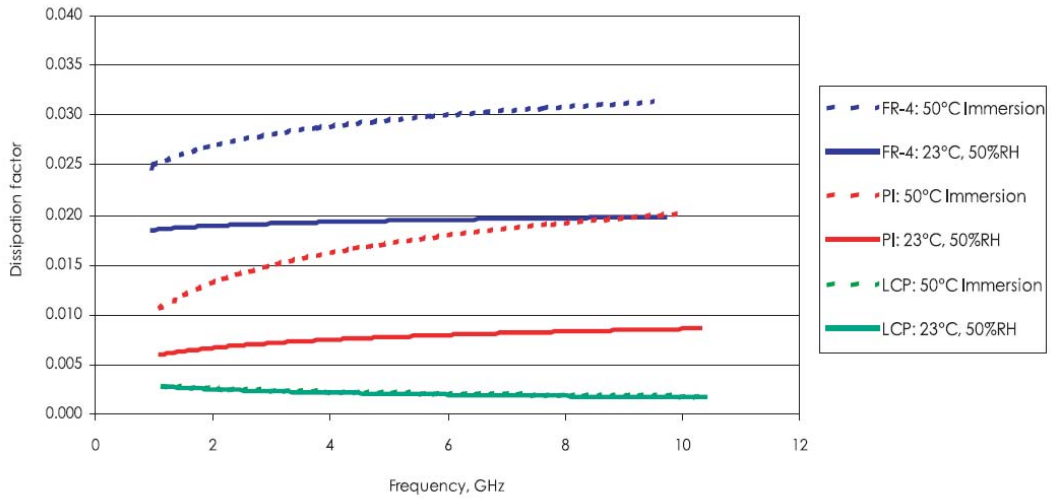
The resistor can be scaled in size in such a way that the quarter wave lines of the Wilkinson divider can wrap around it while avoiding mutual coupling.

Beam steering in the x-direction was achieved by changing the phase difference between the arrays' rows. This was done using integrated SiGe phase shifters. For an 8x8 array, eight phase shifters were used; one per 8x1 row. A beam steering of  $\pm 26^\circ$  off broadside was achieved with grating lobes below -10 dB. The measured radiation patterns at different phase shift values closely match the simulations. Future work to expand this research includes non-uniform feeding of the antenna arrays using a binomial distribution to further reduce side lobe levels. This can be done using embedded planar attenuators to taper the amplitude of individual elements, and has been demonstrated in [3]. Another beneficial addition to this research would be dual polarization of the antenna elements, which increases the beam scanning capabilities. This can be achieved by having two feed lines at  $90^\circ$  of each other and has been demonstrated in [23].

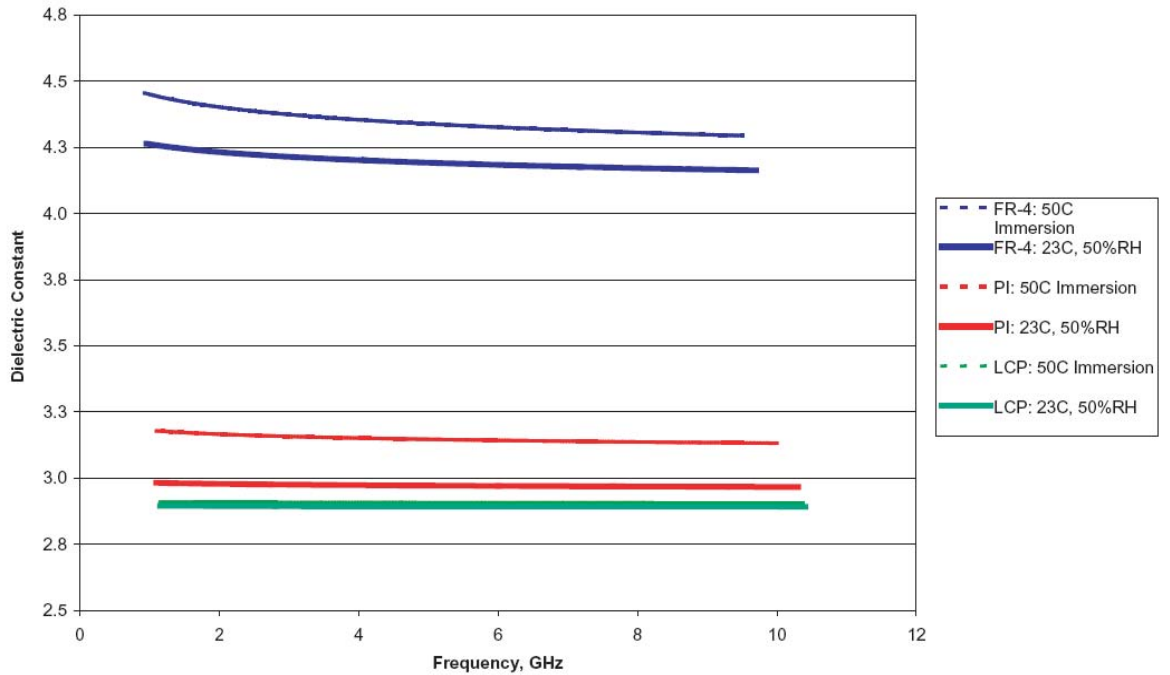
# APPENDIX A

## ELECTRICAL PROPERTIES OF LCP VS. OTHER LAMINATES

Dissipation Factor Variation: LCP, All Polyimide, and FR-4 laminates

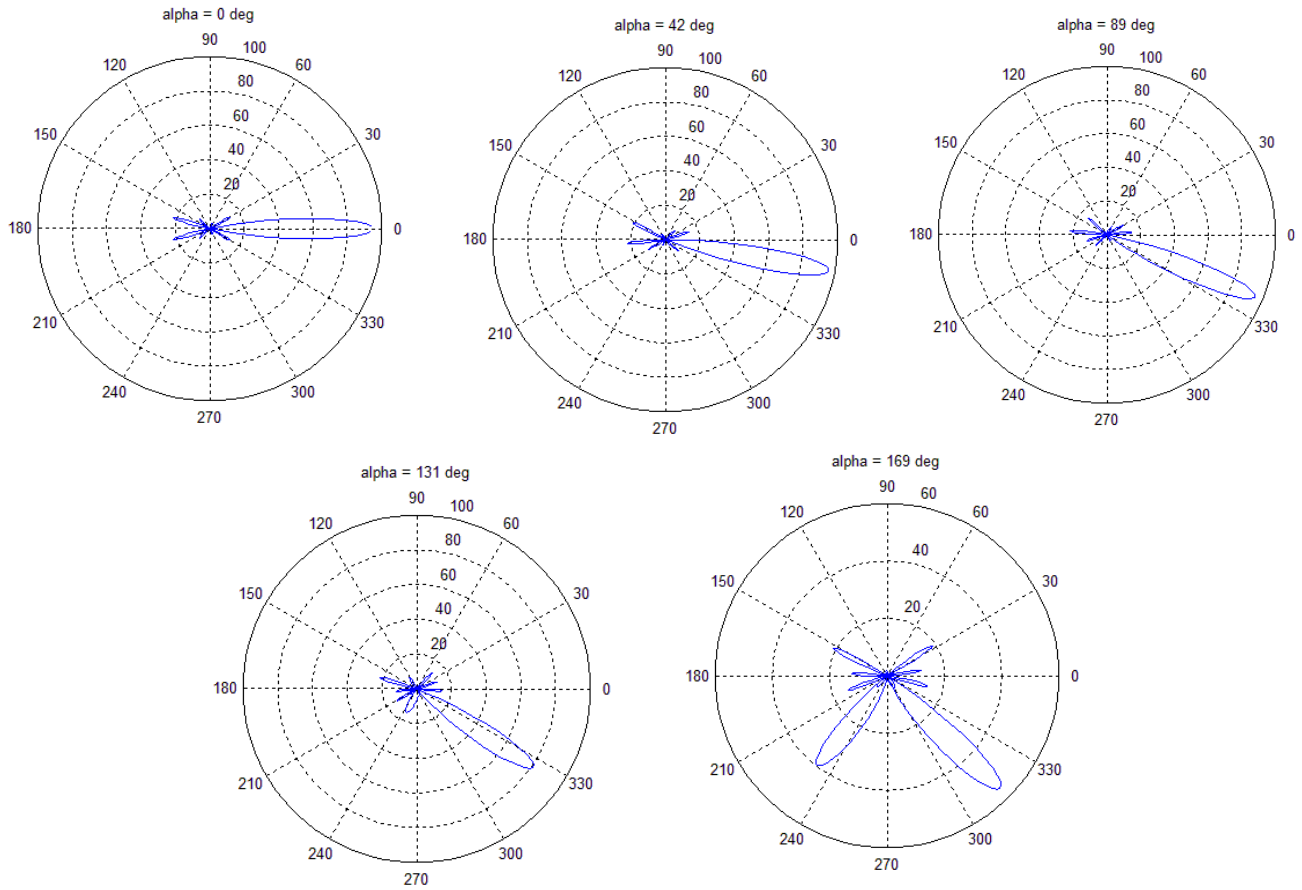


Dielectric Constant Variation: LCP, All Polyimide, and FR-4 laminates



## APPENDIX B

### PREDICTED BEAM STEERING OF 8X8 ARRAY FOR DIFFERENT PHASE SHIFT VALUES



## REFERENCES

- [1] C.A. Balanis, *Antenna Theory Analysis and Design*, 2<sup>nd</sup> ed., New York: John Wiley & Sons, 1997
- [2] "IEEE standard definitions of terms for antennas," *Antennas and Propagation, IEEE Transactions on*, vol.17, no.3, pp. 262- 269, May 1969
- [3] Horst, S.; Anagnostou, D.E.; Ponchak, G.E.; Tentzeris, E.; Papapolymerou, J., "Beam-Shaping of Planar Array Antennas Using Integrated Attenuators," *Electronic Components and Technology Conference, 2007. ECTC '07. Proceedings. 57th*, pp.165-168, May 29 2007-June 1 2007
- [4] Min, S.H.; Seo, C.S.; Yepes, A.M.; Ward, C.; Dalmia, S.; White, G.; Swaminathan, M.; "RF Design Methodology for Design-Cycle-Time Reduction using Parameterization of Embedded Passives on Multilayer Organic Substrates," *Microwave Symposium Digest, 2008 IEEE MTT-S International*, pp.1397-1400, 15-20 June 2008
- [5] T.A. Milligan, *Modern Antenna Design*, 2<sup>nd</sup> ed., Hoboken, NJ: John Wiley & Sons, 2005, Ch. 6
- [6] D.M. Pozar, *Microwave Engineering*, 3<sup>rd</sup> ed., Singapore: John Wiley & Sons, 1989, Ch. 3
- [7] Pozar, D.M.; "Microstrip antennas," *Proceedings of the IEEE*, vol.80, no.1, pp.79-91, Jan 1992
- [8] Rogers Corporation, "ULTRALAM® 3000 Liquid Crystalline Polymer Circuit Material," data sheet available at:  
<http://www.rogerscorp.com/acm/products/17/ULTRALAM-3000-Series-Liquid-Crystalline-Polymer-Circuit-Materials.aspx>
- [9] Rogers Corporation, "RT/duroid® 5880LZ High Frequency Laminates," data sheet available at:  
<http://www.rogerscorp.com/acm/products/10/RT-duroid-5870-5880-5880LZ-High-Frequency-Laminates.aspx>

- [10] Thompson, D.C.; Tantot, O.; Jallageas, H.; Ponchak, G.E.; Tentzeris, M.M.; Papapolymerou, J.; "Characterization Of Liquid Crystal Polymer (LCP) Material and Transmission Lines on LCP Substrates from 30 to 110 GHz," *Microwave Theory and Techniques, IEEE Transactions on* , vol.52, no.4, pp. 1343- 1352, April 2004
- [11] S.J. Horst, "Low Cost Fabrication Techniques for Embedded Resistors on Flexible Organics at Millimeter Wave Frequencies," Master's Thesis, Georgia Institute of Technology, 2006
- [12] S. Haider, "Microstrip Patch Antennas for Broadband Indoor Wireless Systems," Project Report, University of Auckland, 2003
- [13] Sankarasubramaniam, A.; Shastry, P.N.; Katragadda, K., "Design Guidelines for Tunable Coplanar and Microstrip Patch Antennas," *Microwave Integrated Circuit Conference, 2007. EuMIC 2007. European*, pp.504-507, 8-10 Oct. 2007
- [14] Chung, D.J.; Bhattacharya, S.; Ponchak, G.; Papapolymerou, J.; "A Stitching Technique for Expanding Large 3-D Multi-Layer Antenna Arrays in Ku-Band using Small Array Units," *Electronic Components and Technology Conference, 2008. ECTC 2008. 58th*, pp.175-178, 27-30 May 2008
- [15] Horst, S.; Bhattacharya, S.; Tentzeris, M.; Papapolymerou, J.; "Monolithic Low Cost Ka-Band Wilkinson Power Dividers on Flexible Organic Substrates," *Electronic Components and Technology Conference, 2007. ECTC '07. Proceedings. 57th*, pp.1851-1854, May 29 2007-June 1 2007
- [16] Yepes, A.; Bhattacharya, S.; Papapolymerou, J.; "Multilayer Organic X-Band Antenna Arrays Using Wilkinson Power Dividers with Embedded Thin Film Resistors", will be presented at the *2010 IEEE International Symposium on Antennas and Propagation*
- [17] Patterson, C.E.; Thrivikraman, T.K.; Yepes, A.M.; Bhattacharya, S.K.; Cressler, J.D.; and Papapolymerou, J.; "A lightweight X-band organic antenna array with integrated SiGe amplifier," *IEEE Radio & Wireless Symposium*, pp. 84-87, January 2010
- [18] Patterson, C.E.; Thrivikraman, T.K.; Yepes, A.M.; Bhattacharya, S.K.; Cressler, J.D.; and Papapolymerou, J.; "Implementation of a Low Cost, Lightweight X-Band Antenna with Integrated SiGe RF Electronics," *IEEE International Geoscience and Remote Sensing Symposium*, 2010

- [19] Patterson, C.E.; Thirvikraman, T. K.; Yepes, A. M.; Begley, S.M.; Bhattacharya, S. K., Cressler, J. D.; Papapolymerou, J.; "A Lightweight Organic X-Band Phased Array with Integrated SiGe Amplifiers and Phase Shifters", *IEEE Transactions on Antennas and Propagation*, 2009
- [20] Billstrom, N.; Axelsson, K.; Lumetzberger, B.; "X-band Sub-Antenna for Low Cost AESA Radars," *Microwave Conference, 2009. EuMC 2009. European*, pp.910-913, Sept. 29 2009-Oct. 1 2009
- [21] NASA Earth Science Enterprise: Cold Land Processes Working Group, "Parametric Evaluation of Cold-land Processes Measurement Technologies," Final Report, Sep. 2003
- [22] Horst, S.; Bairavasubramanian, R.; Tentzeris, M.M.; Papapolymerou, J., "Modified Wilkinson Power Dividers for Millimeter-Wave Integrated Circuits," *Microwave Theory and Techniques, IEEE Transactions on*, vol.55, no.11, pp.2439-2446, Nov. 2007
- [23] DeJean, G.; Bairavasubramanian, R.; Thompson, D.; Ponchak, G.E.; Tentzeris, M.M.; Papapolymerou, J.; "Liquid Crystal Polymer (LCP): A New Organic Material for the Development of Multilayer Dual-Frequency/Dual-Polarization Flexible Antenna Arrays," *Antennas and Wireless Propagation Letters, IEEE* , vol.4, pp. 22-26, 2005